

MirrorMark: A Distortion-Free Multi-Bit Watermark for Large Language Models

Ya Jiang^{1,2} Massieh Kordi Boroujeny² Surender Suresh Kumar² Kai Zeng²

Abstract

As large language models (LLMs) become integral to applications such as question answering and content creation, reliable content attribution has become increasingly important. Watermarking is a promising approach, but existing methods either provide only binary signals or distort the sampling distribution, degrading text quality; distortion-free approaches, in turn, often suffer from weak detectability or robustness. We propose MirrorMark, a multi-bit and distortion-free watermark for LLMs. By mirroring sampling randomness in a measure-preserving manner, MirrorMark embeds multi-bit messages without altering the token probability distribution, preserving text quality by design. To improve robustness, we introduce a context-based scheduler that balances token assignments across message positions while remaining resilient to insertions and deletions. We further provide a theoretical analysis of the equal error rate to interpret empirical performance. Experiments show that MirrorMark matches the text quality of non-watermarked generation while achieving substantially stronger detectability: with 54 bits embedded in 300 tokens, it improves bit accuracy by 8–12% and correctly identifies up to 11% more watermarked texts at 1% false positive rate.

1. Introduction

The rapid proliferation of large language models (LLMs) such as ChatGPT (OpenAI, 2022), LLaMA (Touvron et al., 2023), and Gemini (Team et al., 2023) has enabled high-quality text generation for tasks including question answering, content creation, and programming assistance (Jo, 2023; Austin et al., 2021; Perkins, 2023). Alongside these

¹Department of Computer Science, George Mason University, Fairfax, VA, USA ²Wireless Cyber Center, College of Engineering and Computing, George Mason University, Fairfax, VA, USA. Correspondence to: Ya Jiang <yjiang25@gmu.edu>.

advances, however, LLMs raise growing concerns regarding the authenticity, ownership, and responsible use of generated content. As synthetic text becomes increasingly indistinguishable from human-written material, content attribution has emerged as a critical mechanism for mitigating misinformation, protecting intellectual property, and enabling accountability in AI deployment (Chandra et al., 2024; Zhao et al., 2025a).

Watermarking has emerged as one of the most promising strategies for verifying the provenance of LLM-generated content, by embedding imperceptible signals into generated outputs that can later be detected. Most existing LLM watermarking methods are designed to answer a binary question: whether a piece of content is watermarked (Kirchenbauer et al., 2023; Aaronson & Kirchner, 2022; Christ et al., 2024; Kuditipudi et al., 2024; Dathathri et al., 2024; Hu et al., 2024; Wu et al., 2024; Liu et al., 2024; Zhao et al., 2025b; He et al., 2025). Importantly, these schemes typically do not require access to the model or the prompt at detection time. Zero-bit watermarking methods can be broadly grouped into three categories. First, distortion-based reweighting approaches bias token logits (e.g., via context-seeded green/red partitions), thereby shifting the model’s output distribution (Kirchenbauer et al., 2023; Zhao et al., 2024; Liu et al., 2024; Zhao et al., 2025b). Second, unbiased reweighting strategies apply step-wise reweighting while preserving the original distribution in expectation (Hu et al., 2024; Wu et al., 2024). Third, distortion-free approaches embed the watermark during the sampling stage, ensuring that the token distribution remains unchanged by design (Aaronson & Kirchner, 2022; Christ et al., 2024; Kuditipudi et al., 2024; Dathathri et al., 2024; He et al., 2025). A detailed discussion of zero-bit watermarking techniques is provided in the Appendix A.1.

While zero-bit watermarking is effective for provenance verification, its binary nature precludes encoding metadata such as model identity, generation time, or usage context. This limitation has motivated growing interest in multi-bit watermarking, which embeds a payload of information to enable richer attribution for auditing and forensic analysis. Existing multi-bit schemes can be broadly categorized into distortion-based methods (Wang et al., 2024; Yoo et al.,

2024; Qu et al., 2024; Jiang et al., 2025), which explicitly bias the output distribution of model to embed information, and distortion-free methods (Zamir, 2024; Kordi Boroujeny et al., 2024), which preserve the original distribution by design. While distortion-based approaches may degrade text quality, existing distortion-free schemes primarily focus on enabling multi-bit embedding and build on watermarking frameworks whose robustness remains an open question (Christ et al., 2024), without incorporating explicit defenses against editing attacks.

A naive multi-key extension encodes multi-bit messages by assigning an independent secret key to each message value and applying a zero-bit watermark under the selected key. While intuitive, this approach does not explicitly construct opposing hypotheses, so mismatched keys behave as independent noise. Therefore, the separation between the matched-key and mismatched-key score distributions is not maximized, limiting the achievable capacity under a constrained token budget. Furthermore, instead of maintaining multiple independent keys, Three-Bricks (Fernandez et al., 2023) derives all message hypotheses from a shared random source via cyclic shifts, extending the schemes of KGW (Kirchenbauer et al., 2023) and AA (Aaronson & Kirchner, 2022) to multi-bit watermarking. Concretely, in the extension of AA, a single key generates a random vector, and embedding an m -bit message $M \in \{0, \dots, 2^m - 1\}$ corresponds to assigning random values starting from the M -th entry of this vector to the vocabulary tokens, enabling efficient 2^m -way identification. However, this formulation treats multi-bit decoding as a multi-class hypothesis testing problem, where different messages correspond to shifted but otherwise symmetric hypotheses. As the message space grows, multiple-testing correction becomes increasingly stringent, and cyclic shifts alone do not maximize the statistical separation between the true message and incorrect alternatives, limiting capacity and bit accuracy under a constrained token budget.

Similarly, RSBH (Qu et al., 2024) employ message-dependent cyclic shifts based on KGW and bias tokens in the corresponding green list to facilitate multi-bit decoding, further incorporating error-correcting codes to improve robustness. However, since cyclic shifts do not inherently provide strong hypothesis separation, reliable decoding requires applying a strong bias to amplify the signal. For example, RSBH sets the bias parameter to $\delta = 6.0$ to achieve high bit accuracy, at the cost of substantially increased text distortion. In contrast, MirrorMark employs a single-key and structured mirroring construction that explicitly maximizes the contrast between the true message and all incorrect hypotheses. By designing mutually dependent and complementary score distributions, MirrorMark achieves stronger separation per token, leading to higher bit accuracy than ThreeBricks.

In this work, we introduce MirrorMark, a framework that extends the distortion-free sampling paradigms of AA (Aaronson & Kirchner, 2022) and SynthID (Dathathri et al., 2024) to enable multi-bit watermarking without altering the token distribution. By mirroring sampling randomness in a measure-preserving manner, MirrorMark embeds multi-bit messages while preserving text quality, and achieves substantially stronger detectability than state-of-the-art methods. To improve robustness against editing attacks, we propose the Context-Anchored Balanced Scheduler (CABS), which anchors watermark scheduling to context-hashed frames and enforces balanced token assignment across message positions, mitigating the effects of token insertions and deletions. We further develop a theoretical characterization of the equal error rate (EER), providing interpretability for the observed empirical behavior. We conduct a comprehensive evaluation against MPAC (Yoo et al., 2024), RSBH (Qu et al., 2024), and StealthInk (Jiang et al., 2025). In addition, we include the Gumbel-max-based multi-bit construction of Three-Bricks (Fernandez et al., 2023) as a controlled baseline to highlight the benefit of structured multi-bit encoding under the same sampling paradigm. With 36 bits embedded in 300 tokens, MirrorMark achieves up to 100% TPR at 1% FPR and over 98% bit accuracy, with text quality comparable to non-watermarked text.

2. Warm up: AA (Aaronson & Kirchner, 2022) and SynthID (Dathathri et al., 2024)¹

The zero-bit watermarking methods that can be extended to multi-bit using MirrorMark are those that generate the next token by sampling a random value. In this paper, we select two representatives, i.e., AA and SynthID to apply MirrorMark. In this section, we introduce their basic ideas. Let $p(x_1), \dots, p(x_V)$ denote the probability distribution over the V -tokens vocabulary at generation step t , given by the LLM as $p_{\text{LM}}(\cdot | x_{<t})$.

2.1. Gumbel-max Sampling

The classical Gumbel trick (Gumbel, 1954) samples from this distribution by adding i.i.d. Gumbel(0, 1) noise to the log-probabilities:

$$x^* = \arg \max_i \{ \log p(x_i) + G_i \}, \quad (1)$$

which guarantees $\Pr(x^* = x_i) = p(x_i)$. Using the representation $G_i = -\log(-\log U_i)$ with $U_i \sim \text{Uniform}(0, 1)$,

¹In our paper, uppercase characters such as G , U denote the random variable, while lowercase character such as u denotes the realization of the random variables, and bold character such as \mathbf{u} denotes vectors.

this is equivalently

$$\begin{aligned} x^* &= \arg \max_{1 \leq i \leq V} [\log p(x_i) - \log(-\log U_i)] \\ &= \arg \max_{1 \leq i \leq V} U_i^{1/p(x_i)}. \end{aligned} \quad (2)$$

To embed the watermark by Gumbel-max sampling, at step t , AA use watermark key and the context tokens as the seed r_t and set $u_i = g(x_i, r_t)$ for token x_i where $g(\cdot, r_t)$ is a pseudorandom function (PRF) with range $\text{Uniform}(0, 1)$. This construction ensures that the watermark is embedded in the sampled token and can later be detected by reproducing these pseudorandom draws and designing an appropriate score function. Besides, due to the property of gumbel trick, the sampling process is distortion-free. However, as equation 2 shows, the token with the largest $U_i^{1/p(x_i)}$ is always selected. Therefore, the generated response is deterministic for the same prompt.

2.2. Tournament Sampling

SynthID proposes tournament sampling to embed a zero-bit watermark. Tournament sampling proceeds in L layers. At layer ℓ , a PRF $g^\ell(\cdot, r_t) : \mathcal{V} \rightarrow [0, 1]$ assigns each token a value u^ℓ using a seed r_t from the watermark key and context tokens. Before the tournament starts, n_0 candidate tokens $\{c_1, \dots, c_{n_0}\}$ are sampled from original probability distribution $p_{\text{LM}}(\cdot | x_{<t})$. In particular, with L layers, $n_0 = 2^L$. For the first layer $\ell = 1$, the n_0 candidates are randomly paired. For each subsequent layer $\ell = 2, \dots, L$, the $n_{\ell-1}$ surviving candidates are paired according to the tournament structure. In each match, the token with larger g -value wins. The winners form the candidate set for the next layer. After L layers, the remaining single token x_t is chosen as the output token. Compared to AA which deterministically samples the token, the method in SynthID is a probabilistic scheme. Therefore, the responses generated by SynthID will show more diversity.

2.3. Detection

Given a text x_1, \dots, x_T , the detector in AA recomputes $u_t = g(x_t, r_t)$ for $t = 1, \dots, T$. If the text is not watermarked, the u_t values follow $\text{Uniform}(0, 1)$ i.i.d.; if watermarked, they are skewed toward larger values. AA proposed equation 3 to calculate the score for the text as,

$$\text{LogScore}(x) = - \sum_{t=1}^T \log(1 - u_t). \quad (3)$$

Following SynthID, let $u_{t,\ell} := g^\ell(x_t, r_t)$ denote the score produced by the ℓ -th layer at step t , and let α_ℓ be the corresponding layer weight. The overall detection statistic is defined as the weighted mean score

$$\text{WeightedMeanScore} = \frac{1}{TL} \sum_{t=1}^T \sum_{\ell=1}^L \alpha_\ell u_{t,\ell}, \quad (4)$$

Furthermore, by accounting for the multi-layer structure, they leverage a Bayesian score that aggregates evidence across tokens and layers, i.e.,

$$\begin{aligned} \text{BayesianScore}(x) &= P(w | \mathbf{u}) = \sigma \left(\log \frac{P(w | \mathbf{u})}{P(\neg w | \mathbf{u})} \right) \\ &= \sigma \left(\log \frac{P(\mathbf{u} | w)}{P(\mathbf{u} | \neg w)} + \log \frac{P(w)}{1 - P(w)} \right), \end{aligned} \quad (5)$$

where $P(w)$ and $P(\neg w)$ are respectively watermarked and nonwatermarked priors, $P(w | \mathbf{u})$ is the watermarked posterior, while $P(\mathbf{u} | w)$ and $P(\mathbf{u} | \neg w)$ are the likelihood for the watermarked and non-watermarked hypotheses, respectively, and $\sigma(\cdot)$ is the logistic sigmoid. Since $u_{t,\ell}$ is a value generated by a PRF following $\text{Uniform}(0, 1)$, referring to equation A7 in SynthID,

$$P(\mathbf{u} | \neg w) = \prod_{t=1}^T \prod_{\ell=1}^L P(u_{t,\ell} | \neg w) = \prod_{t=1}^T \prod_{\ell=1}^L 1 = 1, \quad (6)$$

Referring to equations A8, A9, and A10 in SynthID,

$$\begin{aligned} P(\mathbf{u} | w) &= \prod_{t=1}^T \prod_{\ell=1}^L P(u_{t,\ell} | w, u_{t,<\ell}) \\ &= \prod_{t=1}^T \prod_{\ell=1}^L \sum_{c=1}^2 P(u_{t,\ell} | \pi_{t,\ell} = c) P(\pi_{t,\ell} = c | w, u_{t,<\ell}), \end{aligned} \quad (7)$$

where $\pi_{t,\ell}$ denotes the number of distinct u values in the pairwise tournament at layer ℓ for t -th token, and hence $\pi_{t,\ell} \in \{1, 2\}$. They derive $P(u_{t,\ell} | \pi_{t,\ell} = c)$ following the analysis in SynthID [Eq. A9] as the distribution of watermarked $u_{t,\ell}$ given $\pi_{t,\ell}$. Since the number of unique u values is governed by the layer entropy and can be predicted from the preceding u values, i.e., higher-entropy time steps typically produce larger u values. Therefore, they used a logistic regression model to predict $P(\pi_{t,\ell} = c | w, u_{t,<\ell})$.

3. MirrorMark

In this paper, we propose a multi-bit and distortion-free watermarking framework, MirrorMark, which combines three complementary components to embed and recover multi-bit messages without altering the output distribution of LLMs. First, a mod-1 mirroring transformation encodes an m -bit symbol by reflecting each u value around a message-specific pivot. Next, the Context-Anchored Balanced Scheduler (CABS) determines which symbol is embedded at each generation step by mapping tokens to message positions in a balanced and context-dependent manner. Finally, during decoding, CABS is replayed to recover token-to-position assignments, each symbol is decoded from the mirrored u values using the appropriate score function, and all decoded values over the tokens are aggregated to detect the watermark.

3.1. Mod-1 Mirroring

To extend AA and SynthID to multi-bit watermarking, we propose a mod-1 mirroring process and denote an m -bit watermark message as $M \in \mathbb{M} = \{0, 1, \dots, 2^m - 1\}$. Let $U \sim \text{Uniform}(0, 1)$ and let $u \in [0, 1)$ denote a realization of U , corresponding to the sampling procedures in Sections 2.1 and 2.2. We define the mirroring point $\psi_M = \frac{M}{2^{m+1}}$ and reflect u about ψ_M as follows:

$$\Psi(u; \psi_M) = (2\psi_M - u) \bmod 1. \quad (8)$$

For clarity, the mod-1 mirroring operation in equation 8 can be equivalently written in a piecewise form:

$$\Psi(u; \psi_M) = \begin{cases} 2\psi_M - u + 1, & \text{if } -1 < 2\psi_M - u < 0, \\ 2\psi_M - u, & \text{if } 0 \leq 2\psi_M - u < 1. \end{cases} \quad (9)$$

This formulation explicitly shows how the reflection is wrapped back into the unit interval $[0, 1)$ through the modulo operation. Fig. 4 in Appendix B illustrates the mod-1 mirroring process for the 1-bit and 2-bit cases, respectively. The map $u \mapsto (2\psi - u) \bmod 1$ is a measure-preserving involution on $[0, 1)$ because it is a bijection that preserves local lengths. Hence, if $U \sim \text{Uniform}(0, 1)$, then $\Psi(U; \psi) \sim \text{Uniform}(0, 1)$. To embed the watermark, the encoder uses the mirrored u corresponding to the chosen message M to draw the next token.

Remark (1-bit mod-1 mirroring case). When $m = 1$, we adopt a slightly specialized form of mod-1 mirroring for analytical convenience,

$$\Psi(u; M) = \begin{cases} 1 - u, & M = 0, \\ u, & M = 1. \end{cases} \quad (10)$$

It enforces the complementary property $\Psi(u; 0) + \Psi(u; 1) \equiv 1$ per token, which is explicitly used in the derivation of tournament-based MirrorMark in Appendix F.2. Importantly, it does not change the geometric structure of mod-1 mirroring, and the induced partition and mapping of the unit interval are identical to $m = 1$ under 8, shown as Fig. 4a. Meanwhile, the a little bit stronger separation between mirrored values under this symmetric form (e.g., $u = 0.2$ mapping to 0.8 versus 0.2 under equation 10, rather than 0.8 versus 0.3 with under equation 8) could also lead to a slight improvement in bit accuracy.

3.2. Context-Anchored Balanced Scheduler (CABS)

To embed more bits in limited tokens, similar to MPAC (Yoo et al., 2024) and StealthInk (Jiang et al., 2025), we construct a message sequence MsgSeq with H positions², where each position is intended to carry an m -bit symbol, and in this way we embed a payload of $b = m \cdot H$

² $\text{MsgSeq} \in \{0, \dots, 2^m - 1\}^H$, which means each position of MsgSeq carries an m -bit symbol.

bits. In their methods, during generation, an m -bit symbol to be embedded is assigned to the next token by pseudorandomly selecting a position based on the watermark key and the context tokens. However, such pseudorandom allocation does not guarantee uniform token distribution across positions with limited number of tokens. For instance, some positions may not receive any tokens at all, in which case the embedded message must be guessed at random during decoding. An intuitive alternative is to preferentially assign tokens to positions that are underrepresented. Yet, this strategy is fragile: even a few token insertions or deletions can desynchronize the assigned positions from those used at generation, thereby destroying the watermark.

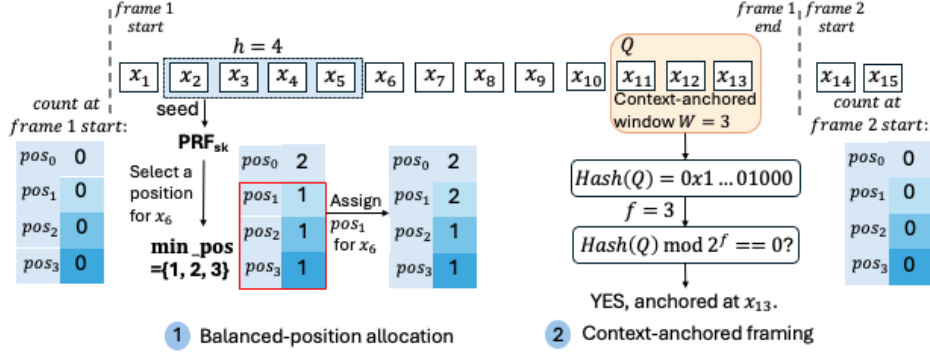
To address these challenges, we propose a context-anchored balanced scheduler (CABS), which aims to balance token assignments across positions while maintaining robustness against desynchronization. We present CABS as in Fig. 1 and formally in Algorithm 1 in Appendix C. Specifically, CABS has two components: balanced-position allocation and context-anchored framing. To achieve balanced-position allocation, CABS maps token to a position based on context h tokens, ensuring that each position receives a sufficient number of tokens for reliable decoding, while avoiding reliance on fragile sequential assignments. Importantly, assignments are performed within frames, and each frame boundary is determined by a context-anchored window Q of W tokens. A new frame is anchored whenever the f least significant bits of $\text{Hash}(Q)$ are all zero. At the start of each frame, the token counts for all positions are reset, and the allocation restarts from a synchronized state. This framing mechanism prevents error propagation across the entire sequence and confines the impact of local insertions or deletions to the affected frame. Besides, the parameters min_len and max_len shown in Algorithm 1 restrict the frame length between successive anchors, so that no frame is too short which avoids instability, or too long which prevents unbounded propagation of insertions or deletions. As a result, CABS not only reduces the risk of empty or highly imbalanced allocations but also improves resilience to editing operations such as insertion, deletion, and substitution. Furthermore, we show the encoding process as Algorithm 2 in Appendix D.

3.3. Decoding and Detection

Since we leverage CABS to allocate each token to a certain position of MsgSeq , each token carries the symbol at that position. We first decode the symbol at each position, and then perform the detection based on decoded MsgSeq .

3.3.1. GUMBEL-MAX-BASED MIRRORMARK

For the Gumbel-max-based construction, we decode the symbol at each position by computing the LogScore for each $M \in \mathbb{M}$ and selecting the maximum. The symbol


 Figure 1: Overview of CABS, where the number of positions $H=4$

at a certain position with assigned K tokens is

$$\hat{M} = \arg \max_{M \in \mathbb{M}} - \sum_{i=1}^K \log (1 - \Psi(u_i, \psi_M)). \quad (11)$$

3.3.2. TOURNAMENT-BASED MIRRORMARK

For the tournament-based construction, we can employ either the WeightedMeanScore or Bayesian decoder to decode the symbol at each position. By comparing the WeightedMeanScore for each $M \in \mathbb{M}$, we can decode the symbol with the maximum score at a certain position allocated with K tokens,

$$\hat{M} = \arg \max_{M \in \mathbb{M}} \frac{1}{K} \sum_{t=1}^K \frac{1}{L} \sum_{\ell=1}^L \alpha_{\ell} \Psi(u_{t,\ell}, \psi_M). \quad (12)$$

For Bayesian decoder, we train a decoder that evaluates the posterior

$$P(M | U, w) \propto P(M) P(U | M, w), \quad (13)$$

where $P(M)$ is the prior and $P(U | M, w)$ is the likelihood of the observed group $U = \{u_{i,j}\}_{i=1..K, j=1..L}$ at a position assigned with K tokens. Denote $\lambda_{i,j,c} = P(\Psi(u_{i,j}, \psi_M) | \pi_{i,j} = c) \times P(\pi_{i,j} = c | w, \Psi(u_{i,<j}, \psi_M))$, similar to equation 7, the likelihood becomes

$$P(U | M, w) = \prod_{i=1}^K \prod_{j=1}^L \sum_{c=1}^2 \lambda_{i,j,c}. \quad (14)$$

Then the Bayesian decision rule selects the symbol with the largest score

$$\hat{M} = \arg \max_{M \in \mathbb{M}} \left\{ \log P(M) + \log \prod_{i=1}^K \prod_{j=1}^L \sum_{c=1}^2 \lambda_{i,j,c} \right\}. \quad (15)$$

3.3.3. DETECTION PROCEDURE

After decoding, the u value of each token is mirrored against the recovered symbol. For symbols decoded by equation 11, equation 12, and equation 15, the mirrored values are aggregated into a global score using

LogScore (equation 3), WeightedMeanScore (equation 4), and BayesianScore (equation 5), respectively. The text is declared watermarked if the score exceeds a predefined threshold. We summarize the procedure in Algorithm 3 in Appendix E: it uses the CABS scheduler to assign tokens to positions, applies the chosen decoder at each position, and performs global detection.

4. Theoretical EER for MirrorMark

In this section, we analyze the theoretical equal error rate (EER) in the single-position setting ($H = 1$). MirrorMark uses multiple positions in practice, and the results reported in Section 5 correspond to the $H > 1$ setting. For completeness, Appendix I.1 presents the performance of MirrorMark under varying m with $H = 1$, and the observed trends are fully consistent with the theoretical behavior analyzed in this section.

Theorem 4.1 Consider sequence-level detection over T approximately independent tokens for MirrorMark based on Gumbel-max sampling and tournament sampling, respectively. We derive the theoretical equal error rate (EER) as follows. See proof in Appendix F.

(i) Gumbel-max sampling. For an LLM with the vocabulary size of V , with m bits embedded,

$$\log \text{EER}_{\text{Gumbel}} = -c_1 T \mathcal{H}^2 + c_2 m + o(T \mathcal{H}^2), \quad (16)$$

where $\mathcal{H} \triangleq - \sum_{i=1}^V p_t(i) \log p_t(i)$ and denotes the entropy of the next-token distribution with $p_t(\cdot) = p_{\text{LM}}(\cdot | x_{<t})$, while $c_1 = \frac{1}{2(1+\pi/\sqrt{6})^2}$ and $c_2 = \frac{\ln 2}{1+\pi/\sqrt{6}}$.

(ii) Tournament sampling. For the tournament sampling with L layers, with 1 bit embedded,

$$\log \text{EER}_{\text{tour}} = -\frac{T}{2} \zeta^2(c) - \frac{1}{2} \log 2\pi T - \log \zeta(c). \quad (17)$$

where $\mathbf{c} \triangleq (L, C_{1,\text{wm}}, C_{2,\text{wm}}, \dots, C_{L,\text{wm}})$ denotes the collection of layer-wise collision probabilities. C_{wm}^{ℓ} is de-

fined in Definition 22 in SynthID and represents the collision probability at layer ℓ , with $\ell \in \{1, 2, \dots, L\}$, which is the probability that two samples drawn i.i.d. from the probability distribution of tokens at layer ℓ are the same.

Fig. 2 visualizes the asymptotic equal error rate predicted by Theorem 4.1, where EER_{tour} follows equation 17. For Gumbel-max-based MirrorMark, although the asymptotic expression in equation 16 is derived under the assumption of a large vocabulary size V , our implementation adopts top-100 sampling in order to match the decoding setting of tournament-based MirrorMark, which violates the large- V assumption underlying the approximation in equation 41 of Appendix F. Therefore, $\text{EER}_{\text{Gumbel}}$ is computed using the exact expression in equation 40, where \mathcal{H} denotes the entropy of the truncated top-100 distribution. Empirically, on LLaMA-2-7B (Touvron et al., 2023) with temperature $\tau = 1.0$ and C4 prompts (Raffel et al., 2020), the average next-token entropy after top-100 sampling is $\mathcal{H} \approx 1.7$. Meanwhile, for tournament-based decoding with $L \in 10, 15, 20, 25, 30$, the corresponding $\zeta(c)$ values fall in the range $[0.14, 0.19]$. Accordingly, Fig. 2 highlights regions that cover these empirically relevant regimes, and the theoretical curves consistently indicate that Gumbel-max decoding achieves a lower asymptotic EER than tournament-based decoding.

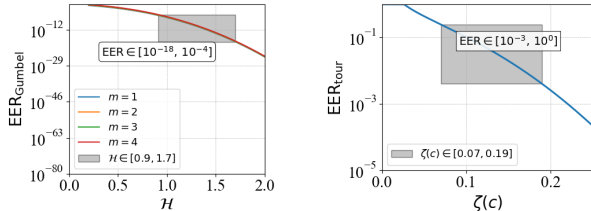


Figure 2: Asymptotic EER of MirrorMark based on Gumbel-max sampling (left) and tournament sampling (right). The token length is set to $T = 200$. For tournament-based MirrorMark, we fix $m = 1$.

5. Evaluations

We compare MirrorMark with three state-of-the-art distortion-based watermarking methods, MPAC (Yoo et al., 2024), RSBH (Qu et al., 2024), and StealthInk (Jiang et al., 2025), evaluating detectability, text quality, and robustness. These baselines modify the token sampling distribution during generation, while StealthInk preserves the distribution in expectation. We additionally include the Gumbel-max-based multi-bit construction of ThreeBricks (Fernandez et al., 2023) as a controlled baseline in Appendix I.1 to highlight the benefit of structured multi-bit encoding under the same sampling paradigm. For MirrorMark, we evaluate three score functions, Gumbel-max (equation 3), Tour-Wmean (equation 4), and Tour-Bayes (equation 5), with symbol size $m = 3$ unless otherwise specified. Experi-

ments are conducted using LLaMA2-7B (Touvron et al., 2023) on 500 prompts sampled from the RealNewsLike subset of C4 (Raffel et al., 2020). We report AUC and TPR@1%FPR for detection, bit accuracy for decoding, and perplexity, GPT-4o score, and repetition rate for text quality. Additional details are provided in Appendix H.

5.1. Alignment with Theorem 4.1

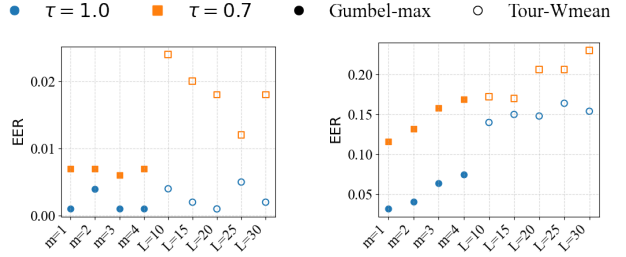


Figure 3: Empirical EER of MirrorMark on LLaMA-2-7B (Touvron et al., 2023) with C4 prompts (Raffel et al., 2020) (left) and Gemma-7B-it (Team et al., 2024) with EL15 prompts (Fan et al., 2019) (right), with token length $T = 200$. For tournament-based MirrorMark, $m = 1$.

Fig. 3 reports empirical EER under a fixed token budget of $T = 200$. The empirical values are higher than the theoretical curves in Fig. 2, which is expected since Theorem 4.1 is asymptotic and assumes approximate token independence, while practical decoding involves token correlations and finite T . In terms of the trend of EER, the empirical results are consistent with Theorem 4.1, where Gumbel-max-based MirrorMark achieves lower EER than tournament-based MirrorMark under the same settings. In addition, we observe that the empirical gap between Gumbel-max and tournament-based decoding depends strongly on the effective entropy induced by the sampling configuration. In the high-entropy regime (e.g., LLaMA-2-7B with $\tau = 1.0$, where the top-100 entropy is relatively high), Gumbel-max and Tour-Wmean achieve comparable EER. When entropy decreases (e.g., $\tau = 0.7$ with $\mathcal{H} \approx 0.91$ and $\zeta(c)$ spanning roughly 0.07–0.16), the advantage of Gumbel-max becomes much more pronounced, and the EER of tournament-based decoding improves more substantially than it does at $\tau = 1.0$. Under even stricter entropy conditions (right plot; e.g., $\mathcal{H} \approx 0.54$ at $\tau = 1.0$ with $\zeta(c) \approx 0.017$ –0.02), the impact of the symbol size m in Gumbel-max becomes evident, with EER increasing as m grows, consistent with the theoretical dependence on m . In contrast, the tournament variant exhibits a stronger sensitivity to the choice of L ; in particular, larger L can lead to noticeably worse EER (e.g., $L = 30$ under both $\tau = 1.0$ and $\tau = 0.7$). This behavior is expected in low-entropy regimes. While increasing the tournament depth L intuitively aggregates more watermark evidence, each additional layer further consumes the limited randomness avail-

Table 1: Mean perplexity and detectability for different approaches on 300 tokens. Each perplexity is reported with a 90% confidence interval based on bootstrapping.

Method	36 Bits				54 Bits			
	AUC	TPR@1%FPR	Bit Acc.	Perplexity	AUC	TPR@1%FPR	Bit Acc.	Perplexity
Non Watermark	–	–	–	7.2784 [7.1294, 7.4296]	–	–	–	7.2784 [7.1294, 7.4296]
MPAC	0.9949	0.9800	0.9347	9.1951 [9.0404, 9.3516]	0.9962	0.9840	0.8928	9.3457 [9.1704, 9.5224]
RSBH	0.9998	0.9980	1.0000	32.8955 [31.4973, 34.3369]	0.9989	0.9980	0.9928	32.8184 [31.3574, 34.3446]
StealthInk	0.9892	0.8520	0.8896	7.8241 [7.6260, 8.0223]	0.9890	0.8900	0.8415	7.8950 [7.6933, 8.0974]
Gumbel-max	1.0	1.0	0.9835	7.0486 [6.8991, 7.1997]	1.0	1.0	0.9683	7.1751 [7.0195, 7.3383]
Tour-Wmean	0.9990	0.9920	0.9732	7.3706 [7.2265, 7.5202]	1.0	1.0	0.9491	7.3295 [7.1828, 7.4792]
Tour-Bayes	0.9992	0.9960	0.9811	7.3706 [7.2265, 7.5202]	1.0	0.9960	0.9576	7.3295 [7.1828, 7.4792]

able during decoding, leading to a higher collision probability and diminishing returns from later layers. As a result, the marginal contribution of deeper layers quickly decreases and can even become detrimental when noise dominates the signal. This effect is particularly pronounced when Uniform(0, 1)-based u values are used in tournament sampling, which are known to induce higher collision probability across layers under constrained entropy. In Appendix I.6, we provide additional evidence on this low-entropy generation showing that making the u values more extreme could improve detectability, further supporting our entropy-based analysis here, while keeping the discussion in this section focused on the multi-bit setting.

5.2. Trade-off between Text Quality and Detectability

We first evaluate all approaches under moderate payload sizes ($b \in \{36, 54\}$) with 300 generated tokens. Table 1 captures both detectability and text quality. Detectability is assessed using AUC, TPR@FPR=1%, and bit accuracy, while text quality is measured by perplexity. For completeness, we also provide results on shorter sequences of 200 tokens and longer sequences of 400 tokens respectively in Table 4 and Table 5 of Appendix I.2.

From these experiments, we observe that baseline methods exhibit a sharp trade-off between text quality and watermark detectability. Specifically, the baselines either suffer from significant perplexity degradation, making the text less natural, or show weakened detection power, confirming their limited applicability in realistic settings. By contrast, MirrorMark consistently achieves strong detection performance while maintaining perplexity at levels comparable to non-watermarked text, even for only 200 tokens, as demonstrated in Table 4. Besides, we evaluate the GPT4o score and repetition rate across these approaches as in Fig. 6 and Table 6 of Appendix I.3, which demonstrates the superior text quality of MirrorMark.

Given that MirrorMark maintains a favorable trade-off in

these settings, we further stress-test it under larger payload sizes ($b \in \{72, 90\}$). The results in Fig. 8 of Appendix I.4 demonstrate that MirrorMark continues to provide competitive detectability while preserving text quality, highlighting its scalability beyond what baseline approaches can achieve. Overall, the Gumbel-max-based MirrorMark achieves a TPR@1%FPR comparable to the tournament-based MirrorMark, while yielding higher bit accuracy than both Tour-Bayes and Tour-Wmean. Tour-Bayes and Tour-Wmean achieve similar true positive rates, with Tour-Bayes offering superior bit accuracy.

5.3. Robustness

To evaluate robustness, we consider copy-paste and paraphrasing attacks. In the copy-paste attack, a fraction ϵ of non-watermarked text is randomly mixed into watermarked text while preserving the total length. For paraphrasing, we rewrite the watermarked text using the paraphrasing model from (Zhang et al., 2020). Table 2 compares the detectability against copy-paste attacks for different approaches on 400 tokens with 36 bits embedded. In particular, $\epsilon = 0$ means no attack and the performance on the clean samples are reported. In particular, here, for MirrorMark, we present the results with symbol size $m = 2$. Besides, we show the results with $\epsilon \in \{0.1, 0.3, 0.5\}$ in Table 8 of Appendix I.7. We observe that MirrorMark demonstrates greater robustness compared to other methods. Furthermore, we examine the robustness under different symbol sizes $m \in \{2, 3, 4, 6\}$ in Fig. 12 and Fig. 13 in Appendix I.7. Setting $m = 2$ yields consistently strong performance. However, while Gumbel-max benefits from $m = 6$, the other two methods do not. When $m = 6$, the number of positions becomes $H = 6$. Although this increases the number of tokens allocated per position, in tournament-based MirrorMark, even without attack, the number of tokens per position is still insufficient to reliably decode 6 bits with high accuracy.

Table 2: Detectability under copy-paste attacks on 400-token texts with 36 embedded bits (ϵ denotes the edit fraction).

Method	$\epsilon = 0$ (No attack)			$\epsilon = 0.2$			$\epsilon = 0.4$		
	AUC	TPR@1%FPR	Bit Acc.	AUC	TPR@1%FPR	Bit Acc.	AUC	TPR@1%FPR	Bit Acc.
MPAC	0.9970	0.9820	0.9599	0.9753	0.8975	0.8997	0.9593	0.7675	0.8397
RSBH	0.9999	1.0	1.0	0.9697	0.0850	0.6138	0.8455	0.0050	0.6038
StealthInk	0.9941	0.9500	0.9204	0.9705	0.8175	0.8448	0.9172	0.4750	0.7716
Tour-Wmean	0.9997	1.0	0.9681	0.9981	0.9900	0.9106	0.9825	0.8980	0.8323
Tour-Bayes	0.9996	1.0	0.9681	0.9978	0.9840	0.9106	0.9900	0.9220	0.8323
Gumbel-max	1.0	1.0	0.9891	1.0	0.9690	1.0	1.0	0.9328	

Table 3: Detectability under paraphrasing attacks for different schemes. TB denotes Tour-Bayes and G-max denotes Gumbel-max. Multi-bit methods embed 36 bits in 400 tokens.

	MPAC	RSBH	StealthInk	TB (0 bit)	TB (m=2)	TB (m=3)	TB (m=4)	TB (m=6)	G-max (0 bit)	G-max (m=2)	G-max (m=3)	G-max (m=4)	G-max (m=6)
AUC	0.5743	0.3414	0.5188	0.7925	0.8139	0.9001	0.8938	0.8140	0.8245	0.9306	0.9091	0.9109	0.9025
TPR@1%FPR	0.0100	0.0000	0.0050	0.2630	0.2220	0.3200	0.3480	0.2300	0.2800	0.5780	0.4860	0.4620	0.3840
Bit Accuracy	0.5734	0.6220	0.5673	–	0.5216	0.5152	0.5152	0.5123	–	0.5434	0.5398	0.5378	0.5333

Table 3 compares the performance under paraphrasing attacks. Overall, MirrorMark maintains strong separability between watermarked and non-watermarked samples in terms of AUC, since paraphrasing changes the surface form of sentences but often preserves underlying semantic and statistical patterns that still carry weak watermark signals. In contrast, all methods exhibit poor bit accuracy. This degradation arises because paraphrasing alters sentence structure and wording in ways that directly disrupt the precise token-level dependencies required for accurate bit recovery. Achieving robustness against paraphrasing attacks therefore remains an open problem in the design of multi-bit watermarking schemes. Interestingly, we observe that MirrorMark achieves better detection rate such as AUC and TPR@1%FPR than its zero-bit baselines (e.g., TB ($m = 4$) vs. TB (0 bit)), and G-max ($m = 2$) vs. G-max (0 bit)).

6. Ablation Study

We first conduct an ablation study on the key parameters of CABS, including frame size f , context window W , and maximum frame expansion factor `max_factor`. The full ablation results under insertion, deletion, and substitution attacks are reported in the Tables 9–11 of Appendix I.8.1.

Across all attack types and edit ratios, we observe consistent trends. In particular, $f = 3$ yields the best overall trade-off between robustness and bit recovery, while $W = 4$ provides sufficient contextual coverage without overfitting to local perturbations. Similarly, `max_factor` = 1.5 achieves the strongest robustness across edit rates. Based on these results, we use $f = 3$, $W = 4$, `max_factor` = 1.5 as the default configuration throughout the paper.

Furthermore, to disentangle the contribution of mod-1 mir-

roring from that of position allocation, we further evaluate different position schedulers combined with multiple watermarking schemes. Specifically, we compare CABS with the schedulers used in MPAC and RSBH, denoted as *NaiveHash* and *DPHash*, respectively. Detailed results under different scheduler settings are reported in Fig. 14–16 of Appendix I.8.2. Across all settings, CABS consistently achieves significantly more balanced token allocation across positions, as quantified by a near-zero Gini score³. This balanced allocation translates into clear improvements in detectability for MirrorMark under both Tour-Bayes and Gumbel-max, outperforming NaiveHash and DPHash across all detection metrics. In contrast, for MPAC, the choice of scheduler has a smaller impact on detectability, with CABS yielding only marginal improvements in bit accuracy. These results highlight that balanced position allocation is critical for MirrorMark to aggregate evidence across positions.

7. Conclusion

We propose MirrorMark, a distortion-free multi-bit watermarking scheme for LLMs. MirrorMark encodes messages via mod-1 mirroring of sampling randomness, preserving the output distribution and text quality. To improve robustness, we introduce CABS, which balances symbol allocation and enables reliable recovery under insertions and deletions. We also provide a theoretical analysis of detection error consistent with empirical results. More broadly, MirrorMark can extend any distortion-free zero-bit method that samples next token via random values. Future work includes strengthening robustness to adversarial paraphrasing and exploring mirroring-based watermarking beyond text.

³https://en.wikipedia.org/wiki/Gini_coefficient

References

Aaronson, S. and Kirchner, H. Watermarking of large language models., 2022. URL <https://www.scottaaronson.com/talks/watermark.ppt>.

Atallah, M. J., Raskin, V., Crogan, M., Hempelmann, C., Kerschbaum, F., Mohamed, D., and Naik, S. Natural language watermarking: Design, analysis, and a proof-of-concept implementation. In *Information Hiding: 4th International Workshop, IH 2001 Pittsburgh, PA, USA, April 25–27, 2001 Proceedings 4*. Springer, 2001.

Atallah, M. J., Raskin, V., Hempelmann, C. F., Karahan, M., Sion, R., Topkara, U., and Triezenberg, K. E. Natural language watermarking and tamperproofing. In *International workshop on information hiding*. Springer, 2002.

Austin, J., Odena, A., Nye, M., Bosma, M., Michalewski, H., Dohan, D., Jiang, E., Cai, C., Terry, M., Le, Q., et al. Program synthesis with large language models. *arXiv preprint arXiv:2108.07732*, 2021.

Chandra, B., Dunietz, J., and Roberts, K. Reducing risks posed by synthetic content an overview of technical approaches to digital content transparency, 2024-11-20 05:11:00 2024. URL https://tsapps.nist.gov/publication/get_pdf.cfm?pub_id=959123.

Christ, M., Gunn, S., and Zamir, O. Undetectable watermarks for language models. In Agrawal, S. and Roth, A. (eds.), *Proceedings of Thirty Seventh Conference on Learning Theory*, volume 247 of *Proceedings of Machine Learning Research*, pp. 1125–1139. PMLR, 30 Jun–03 Jul 2024. URL <https://proceedings.mlr.press/v247/christ24a.html>.

Dathathri, S., See, A., Ghaisas, S., Huang, P.-S., McAdam, R., Welbl, J., Bachani, V., Kaskasoli, A., Stanforth, R., Matejovicova, T., Hayes, J., Vyas, N., Merey, M. A., Brown-Cohen, J., Bunel, R., Balle, B., Cemgil, T., Ahmed, Z., Stacpoole, K., Shumailov, I., Baetu, C., Gowal, S., Hassabis, D., and Kohli, P. Scalable watermarking for identifying large language model outputs. *Nature*, 634(8035):818–823, Oct 2024. ISSN 1476-4687. doi: 10.1038/s41586-024-08025-4. URL <https://doi.org/10.1038/s41586-024-08025-4>.

Fan, A., Jernite, Y., Perez, E., Grangier, D., Weston, J., and Auli, M. ELI5: Long form question answering. In Korhonen, A., Traum, D., and Márquez, L. (eds.), *Proceedings of the 57th Annual Meeting of the Association for Computational Linguistics*, pp. 3558–3567, Florence, Italy, July 2019. Association for Computational Linguistics. doi: 10.18653/v1/P19-1346. URL <https://aclanthology.org/P19-1346/>.

Fernandez, P., Chaffin, A., Tit, K., Chappelier, V., and Furun, T. Three bricks to consolidate watermarks for large language models. In *2023 IEEE International Workshop on Information Forensics and Security (WIFS)*. IEEE, 2023.

Gumbel, E. J. *Statistical theory of extreme values and some practical applications: a series of lectures*, volume 33. US Government Printing Office, 1954.

Hasan, T., Bhattacharjee, A., Islam, M. S., Samin, K., Li, Y.-F., Kang, Y.-B., Rahman, M. S., and Shahriyar, R. Xilsum: Large-scale multilingual abstractive summarization for 44 languages, 2021. URL <https://arxiv.org/abs/2106.13822>.

He, H., Liu, Y., Wang, Z., Mao, Y., and Bu, Y. Theoretically grounded framework for LLM watermarking: A distribution-adaptive approach. In *The Thirty-ninth Annual Conference on Neural Information Processing Systems*, 2025. URL <https://openreview.net/forum?id=CMmKcHFDKL>.

Hu, Z., Chen, L., Wu, X., Wu, Y., Zhang, H., and Huang, H. Unbiased watermark for large language models. In *The Twelfth International Conference on Learning Representations*, 2024. URL <https://openreview.net/forum?id=uWVC5FVidc>.

Jiang, Y., Wu, C., Boroujeny, M. K., Mark, B., and Zeng, K. Stealthink: A multi-bit and stealthy watermark for large language models. In *Forty-second International Conference on Machine Learning*, 2025. URL <https://openreview.net/forum?id=dktpDfUTtj>.

Jo, A. The promise and peril of generative ai. *Nature*, 614 (1):214–216, 2023.

Jovanović, N., Staab, R., and Vechev, M. Watermark stealing in large language models. In *Proceedings of the 41st International Conference on Machine Learning*, 2024.

Kirchenbauer, J., Geiping, J., Wen, Y., Katz, J., Miers, I., and Goldstein, T. A watermark for large language models. In Krause, A., Brunskill, E., Cho, K., Engelhardt, B., Sabato, S., and Scarlett, J. (eds.), *Proceedings of the 40th International Conference on Machine Learning*, volume 202 of *Proceedings of Machine Learning Research*, pp. 17061–17084. PMLR, 23–29 Jul 2023. URL <https://proceedings.mlr.press/v202/kirchenbauer23a.html>.

Kirchenbauer, J., Geiping, J., Wen, Y., Shu, M., Saifullah, K., Kong, K., Fernando, K., Saha, A., Goldblum, M., and Goldstein, T. On the reliability of watermarks for large language models. In *ICLR*, 2024. URL <https://openreview.net/forum?id=DEJIDCmW0z>.

Kordi Boroujeny, M., Jiang, Y., Zeng, K., and Mark, B. Multi-Bit Distortion-Free Watermarking for Large Language Models. *arXiv preprint arXiv:2402.16578*, 2024.

Kuditipudi, R., Thickstun, J., Hashimoto, T., and Liang, P. Robust distortion-free watermarks for language models. *Transactions on Machine Learning Research*, 2024. ISSN 2835-8856. URL <https://openreview.net/forum?id=FpaCL1M02C>.

Liu, A., Pan, L., Hu, X., Li, S., Wen, L., King, I., and Yu, P. S. An unforgeable publicly verifiable watermark for large language models. In *The Twelfth International Conference on Learning Representations*, 2024. URL <https://openreview.net/forum?id=gMLQwKDY3N>.

Montemurro, M. A. and Zanette, D. H. Universal entropy of word ordering across linguistic families. *PLOS ONE*, 6(5):1–9, 05 2011. doi: 10.1371/journal.pone.0019875. URL <https://doi.org/10.1371/journal.pone.0019875>.

OpenAI. ChatGPT: Optimizing language models for dialogue. Website, 2022. <https://openai.com/blog/chatgpt>.

Perkins, M. Academic Integrity considerations of AI Large Language Models in the post-pandemic era: ChatGPT and beyond. *Journal of university teaching & learning practice*, 20(2), 2023.

Qu, W., Yin, D., He, Z., Zou, W., Tao, T., Jia, J., and Zhang, J. Provably Robust Multi-bit Watermarking for AI-generated Text via Error Correction Code. *arXiv preprint arXiv:2401.16820*, 2024.

Raffel, C., Shazeer, N., Roberts, A., Lee, K., Narang, S., Matena, M., Zhou, Y., Li, W., and Liu, P. J. Exploring the limits of transfer learning with a unified text-to-text transformer. *Journal of machine learning research*, 21 (140), 2020.

Shih, F. Y. *Digital watermarking and steganography: fundamentals and techniques*. CRC press, 2017.

Team, G., Anil, R., Borgeaud, S., Alayrac, J.-B., Yu, J., Soricut, R., Schalkwyk, J., Dai, A. M., Hauth, A., Milligan, K., et al. Gemini: a family of highly capable multi-modal models. *arXiv preprint arXiv:2312.11805*, 2023.

Team, G., Mesnard, T., Hardin, C., Dadashi, R., Bhupatiraju, S., Pathak, S., Sifre, L., Rivière, M., Kale, M. S., Love, J., and et al., P. T. Gemma: Open models based on gemini research and technology, 2024. URL <https://arxiv.org/abs/2403.08295>.

Topkara, U., Topkara, M., and Atallah, M. J. The hiding virtues of ambiguity: quantifiably resilient watermarking of natural language text through synonym substitutions. In *Proceedings of the 8th workshop on Multimedia and security*, 2006.

Touvron, H., Martin, L., Stone, K., Albert, P., Almahairi, A., Babaei, Y., Bashlykov, N., Batra, S., Bhargava, P., Bhosale, S., et al. Llama 2: Open foundation and fine-tuned chat models. *arXiv preprint arXiv:2307.09288*, 2023.

Wang, L., Yang, W., Chen, D., Zhou, H., Lin, Y., Meng, F., Zhou, J., and Sun, X. Towards codable watermarking for injecting multi-bits information to LLMs. In *The Twelfth International Conference on Learning Representations*, 2024. URL <https://openreview.net/forum?id=JYu5Flqm9D>.

Wu, Y., Hu, Z., Zhang, H., and Huang, H. Dipmark: A stealthy, efficient and resilient watermark for large language models. In *Proceedings of the 41st International Conference on Machine Learning*, 2024.

Yoo, K., Ahn, W., and Kwak, N. Advancing beyond identification: Multi-bit watermark for large language models. In Duh, K., Gomez, H., and Bethard, S. (eds.), *Proceedings of the 2024 Conference of the North American Chapter of the Association for Computational Linguistics: Human Language Technologies (Volume 1: Long Papers)*, pp. 4031–4055, Mexico City, Mexico, June 2024. Association for Computational Linguistics. doi: 10.18653/v1/2024.naacl-long.224. URL <https://aclanthology.org/2024.naacl-long.224/>.

Zamir, O. Excuse me, sir? Your language model is leaking (information). *arXiv preprint arXiv:2401.10360*, 2024.

Zhang, J., Zhao, Y., Saleh, M., and Liu, P. Pegasus: Pre-training with extracted gap-sentences for abstractive summarization. In *International conference on machine learning*, pp. 11328–11339. PMLR, 2020.

Zhao, X., Ananth, P. V., Li, L., and Wang, Y.-X. Provably robust watermarking for AI-generated text. In *The Twelfth International Conference on Learning Representations*, 2024. URL <https://openreview.net/forum?id=SsmT8a045L>.

Zhao, X., Gunn, S., Christ, M., Fairoze, J., Fabrega, A., Carlini, N., Garg, S., Hong, S., Nasr, M., Tramer, F., Jha, S., Li, L., Wang, Y.-X., and Song, D. SoK: Watermarking for AI-Generated Content . In *2025 IEEE Symposium on Security and Privacy (SP)*, pp. 2621–2639, Los Alamitos, CA, USA, May 2025a. IEEE Computer Society. doi: 10.1109/SP61157.2025.00178. URL <https://doi.ieeecomputersociety.org/10.1109/SP61157.2025.00178>.

Zhao, Z., Liu, X., Jha, S., McDaniel, P., Li, B., and Xiao, C. Can watermarks be used to detect large language model intellectual property infringement for free? In *13th International Conference on Learning Representations, ICLR 2025*, pp. 52368–52384. International Conference on Learning Representations, ICLR, 2025b.

A. Related Work

A.1. Zero-bit watermarking

Due to the discrete linguistic nature of text, designing effective watermarking schemes for digital text remains a challenging problem (Shih, 2017). Early approaches were primarily rule-based, including paraphrasing (Atallah et al., 2002), syntactic restructuring (Atallah et al., 2001), and synonym substitution (Topkara et al., 2006). However, these methods relied on handcrafted transformations and were limited in scalability, naturalness, and robustness. The emergence of LLMs created new opportunities for watermarking because they are generative by nature, producing text token by token under probabilistic distributions. This generative process allows watermarking to be embedded directly in the sampling procedure rather than through post hoc text modifications. For example, KGW (Kirchenbauer et al., 2023) introduces the first watermarking scheme for LLMs and highlighted a key property of reweighting-based watermarking: the watermark can be detected algorithmically without knowledge of the model parameters or access to the LLM API. Their method partitions the vocabulary into red and green token lists using a hash function seeded with the preceding context tokens, and then applies a small bias to the logits of green-list tokens. As a result, the watermarked LLM is more likely to generate green-list tokens. Detection is achieved by reconstructing the same lists and conducting hypothesis testing to evaluate whether a text was generated under the reweighted distribution. Subsequent works strengthened this family along several largely complementary dimensions. In particular, Zhao et al. (2024) and Kirchenbauer et al. (2024) provide formal robustness guarantees against distortion-bounded editing attacks, including insertion, deletion, and substitution. Focusing on deployment where detection must be publicly accessible, Liu et al. (2024) propose an unforgeable publicly verifiable watermark that decouples watermark generation and detection so that verification can proceed without revealing the generation key, mitigating counterfeiting risks in public detection settings. Zhao et al. (2025b) explore whether decoding-time watermarks can support model-level IP infringement detection “for free” (i.e., without modifying training pipelines), and identifies practical failure modes such as query sensitivity and hash-key instability, motivating more reliable infringement-oriented detection proce-

dures. Specifically, by retaining the configurations of red-green list, Hu et al. (2024) and Dipmark Wu et al. (2024) introduce an evolved family of permutation-based reweighting strategies for watermarking which maintains the expected distribution of the text; i.e., they proposed a stealthy or unbiased reweighting strategy for LLM watermarking. However, the detector in (Hu et al., 2024) necessitates access to both the prompt and the output distribution provided by the LLM for a given prompt, which requires the detector possesses knowledge of the prompt used to generate the detected text.

In contrast to distortion-based watermarking, which embeds signals by perturbing token probability distributions, recent works have explored distortion-free approaches based on inverse sampling. For example, Christ et al. (2024) and Kuditipudi et al. (2024) propose generating watermarked text without modifying the underlying distribution. However, the method of (Christ et al., 2024) leaves open the challenge of resilience against text corruption. The scheme of (Kuditipudi et al., 2024), although tailored for robust detection, it depends on hundreds of resampling steps during detection, which is computationally prohibitive for long texts. Beyond inverse sampling, other distortion-free techniques have also emerged. Aaronson & Kirchner (2022) introduce a Gumbel-max sampling-based watermark, while Dathathri et al. (2024) develop SynthID, which embeds watermarks through tournament sampling. Furthermore, He et al. (2025) provides a theoretical framework that characterizes fundamental trade-offs between detectability, distortion, and false positive rate in LLM watermarking, and highlights the need for distribution-adaptive designs to achieve reliable detection under strict constraints.

A.2. Multi-bit watermarking

ThreeBricks (Fernandez et al., 2023) extends the schemes of KGW (Kirchenbauer et al., 2023) and AA (Aaronson & Kirchner, 2022), respectively, by encoding multi-bit messages through cyclic shifts of the vocabulary permutation or sampling randomness according to the target message, enabling efficient multi-bit identification. Similarly, RSBH (Qu et al., 2024) construct message-dependent cyclic shifts of the vocabulary permutation based on KGW and bias tokens in the corresponding green list to facilitate multi-bit decoding, further incorporating error-correcting codes to improve robustness. However, these approaches fundamentally formulate multi-bit recovery as a multi-class identification problem, where different messages correspond to shifted but otherwise symmetric hypotheses. As a result, under a constrained token budget, cyclic shifts alone do not explicitly maximize the statistical separation between the true message and incorrect alternatives, leading to limited decoding reliability as the message space grows.

To compensate for this effect, strong bias is often required to amplify the signal. For example, RSBH sets the bias parameter to $\delta = 6.0$ to achieve high bit accuracy, at the cost of substantially increased text distortion.

In contrast, MirrorMark employs a single-key and structured mirroring construction that explicitly creates complementary hypotheses for multi-bit decoding. By directly maximizing per-token contrast between the true message and all incorrect hypotheses while preserving the sampling distribution, MirrorMark achieves reliable multi-bit decoding with high bit accuracy and maintains text quality.

MPAC (Yoo et al., 2024) introduce a multi-color technique. In this scheme, the pseudorandom vocabulary permutation (seeded by prior tokens) is partitioned into multiple equal-length segments, each represented by a distinct color. Message bits are then encoded by selecting color segments. For example, dividing the vocabulary into four colors requires a 2-bits message to specify a segment. During generation, the logits of tokens within the chosen color segment corresponding to the message are boosted by a fixed bias, steering the next token toward that segment.

Beyond color-based methods, other approaches focus on reducing or eliminating distortion. StealthInk (Jiang et al., 2025) perturbs the distribution at each generation step but designs the watermark such that the overall distribution is preserved in expectation, maintaining fluency and text quality. However, its detectability remains limited. In contrast, Kordi Boroujeny et al. (2024) and Zamir (2024) propose multi-bit schemes that are fully distortion-free, ensuring identical input–output distributions. Yet, because they build on the inverse-sampling framework of (Christ et al., 2024), they inherit its unresolved weakness: resilience to text corruption remains an open challenge, with no practical solution to date.

B. Overview of mod-1 mirroring

We illustrate the intuition behind mod-1 mirroring in Fig. 4. The key idea is to encode different messages by reflecting the sampling randomness around message-dependent centers while preserving the uniform distribution over $(0, 1)$. By visualizing how intervals in the original domain are rearranged under mirroring, Fig. 4 highlights how mod-1 mirroring enables multi-bit encoding through structured transformations of randomness without introducing distributional distortion.

C. CABS Scheduling Algorithm 1

Specifically, the function $\text{Elig}(\cdot)$ in Algorithm 1 specifies the eligibility condition for watermarking a token, i.e., the context h tokens are not repeated for the current genera-

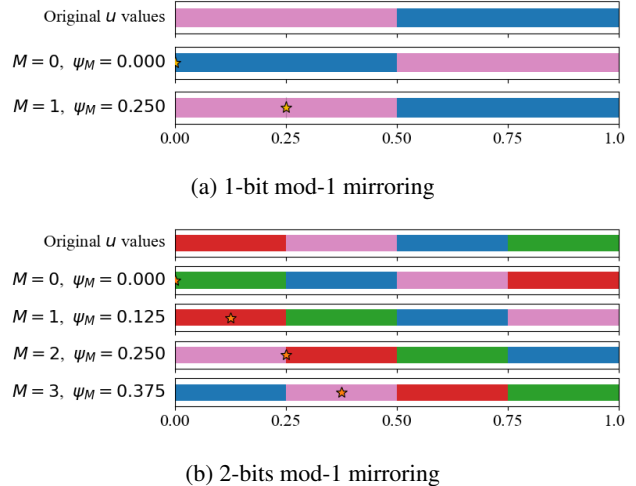


Figure 4: Illustration of mod-1 mirroring under different message capacities, where 1-bit case is based on equation 10, while 2-bits case follows equation 8. In each sub-figure, the first row partitions the original domain $u \in (0, 1)$ into differently colored intervals to illustrate how portions of the domain are transformed. For a given message M , the star marker indicates the mirroring center ψ_M . Applying mod-1 mirroring around ψ_M moves each original interval to a new location within $(0, 1)$. Colors are used only to track this transformation: under a fixed M , all u values that start in the same colored interval in the original row appear together in the interval with the same color after mirroring.

tion step. Since each random value is generated by a PRF seeding the context h tokens, this restriction avoids correlations between consecutive watermarking decisions and helps maintain the statistical independence of the resulting pseudorandom draws.

Algorithm 1 CABS Scheduling

Input: Eligibility function $\text{Elig}(\cdot)$, secret key sk , message length H , counter vector $c \leftarrow \mathbf{0}^H$, queue $Q \leftarrow []$, window size W , f , count of tokens within a frame $\ell \leftarrow 0$, context length h , min_len , max_factor , sequence $\mathbf{x}_{0:T-1}$

Output: Position assignment for each eligible token

```

1:  $\text{max\_len} = \text{max\_factor} \times H$ 
2: for  $i = h, \dots, T-1$  do
3:   if not  $\text{Elig}(\mathbf{x}_{i-h:i-1})$  then
4:     continue
5:   else
6:      $F \leftarrow \text{Hash}(Q)$ 
7:      $Q.\text{enqueue}(\mathbf{x}_i)$ 
8:     if  $|Q| > W$  then
9:        $Q.\text{dequeue}(\mathbf{x}_{i-W})$ 
10:    end if
11:     $\text{min\_pos} = \arg \min(c)$  %% Select the positions with the fewest tokens from counter vector for tokens-to-positions mapping
12:     $pos \sim \text{Unif}(\text{min\_pos})$  %% Randomly select a position, seeded by  $\text{PRF}_{\text{sk}}(\mathbf{x}_{i-h:i-1})$ 
13:     $c_{pos} \leftarrow c_{pos} + 1$  %% Increment the count for the assigned position
14:     $\ell \leftarrow \ell + 1$  %% Increment the count of tokens for the current frame
15:     $cut$  (true or false)  $\leftarrow (\ell \geq \text{min\_len} \wedge (F \bmod 2^f == 0)) \vee (\ell \geq \text{max\_len})$  %% Whether to end the current frame and start a new one
16:    if  $cut$  then
17:       $c \leftarrow \mathbf{0}^H$ ,  $Q \leftarrow []$ ,  $\ell \leftarrow 0$ 
18:    end if
19:  end if
20: end for

```

D. CABS-based Encoder Algorithm 2

E. CABS-based Decoding and Detection Algorithm 3

F. Proof for Theorem 4.1: Theoretical EER of MirrorMark

In the following, we analyze the theoretical EER of Gumbel-max and tournament-based MirrorMark with the

Algorithm 2 CABS-based Encoder

Input: CABS parameters $(\text{sk}, H, W, f, h, \text{min_len}, \text{max_factor})$, prompt \mathbf{a} , length T , message sequence with H positions $\text{MsgSeq} \in \{0, \dots, 2^m - 1\}^H$, original distribution p_{LM} , watermarked distribution p_{wm}

Output: Generated sequence $\mathbf{x}_{0:T-1}$

```

1:  $\text{max\_len} = \text{max\_factor} \times H$ 
2:  $cabs \leftarrow \text{CABS}(\text{sk}, H, W, f, h, \text{min\_len}, \text{max\_len})$ 
3: for  $t = 0$  to  $T-1$  do
4:   if  $t < h$  then
5:     Sample  $x_t \sim p_{LM}(\cdot | \mathbf{a}, \mathbf{x}_{:t-1})$ 
6:   else
7:      $pos \leftarrow cabs(\mathbf{x}_{:t-1})$ 
8:     Sample  $x_t \sim p_{wm}(\cdot | \mathbf{a}, \mathbf{x}_{:t-1}, \text{MsgSeq}[pos])$ 
9:   end if
10: end for

```

Algorithm 3 CABS-based Decoding & Detection

Input: Sequence $\mathbf{x}_{0:T-1}$, secret key sk , message length H , context length h , CABS params $(\text{Elig}(\cdot), W, f, \text{min_len}, \text{max_factor})$, decoder choice $\text{DEC} \in \{\text{gumbel}, \text{wmean}, \text{bayes}\}$, scorer choice $\text{SCORER} \in \{\text{gumbel}, \text{wmean}, \text{bayes}\}$, threshold thres

Output: Message sequence $\text{MsgSeq} \in \{0, \dots, 2^m - 1\}^H$ and a decision $\in \{\text{true}, \text{false}\}$ on whether $\mathbf{x}_{0:T-1}$ is watermarked

```

1:  $\text{max\_len} = \text{max\_factor} \times H$ 
2:  $cabs \leftarrow \text{CABS}(\text{Elig}(\cdot), \text{sk}, H, W, f, h, \text{min\_len}, \text{max\_len})$ 
3: Initialize  $\mathcal{U} \leftarrow \{pos : [] \mid pos = 1, \dots, H\}$ ,  $\mathcal{U}_{\text{mirror}} \leftarrow []$ 
4: for  $t = h, \dots, T-1$  do
5:    $pos \leftarrow cabs(\mathbf{x}_{:t})$ 
6:   Generate random value  $u_t$  seeding  $\text{sk}$  and  $\mathbf{x}_{t-h:t}$ 
7:    $\mathcal{U}[pos].\text{append}(u_t)$ 
8: end for
9: for  $pos = 1, \dots, H$  do
10:   $\text{MsgSeq}[pos] \leftarrow \text{SymbolDecoder}(\mathcal{U}[pos]; \text{DEC})$  %% If  $\text{DEC} = \text{gumbel}$  use equation 11; if  $\text{DEC} = \text{wmean}$  use equation 12; if  $\text{DEC} = \text{bayes}$  use equation 15.
11:  for each  $u \in \mathcal{U}[pos]$  do
12:     $u_{\text{mir}} \leftarrow \Psi(u, \psi_{\text{MsgSeq}[pos]})$ 
13:     $\mathcal{U}_{\text{mirror}}.\text{append}(u_{\text{mir}})$ 
14:  end for
15: end for
16:  $score \leftarrow \text{Score}(\mathcal{U}_{\text{mirror}}; \text{SCORER})$  %% If  $\text{SCORER} = \text{gumbel}$  use equation 3; if  $\text{SCORER} = \text{wmean}$  use equation 4; if  $\text{SCORER} = \text{bayes}$  use equation 5.
17: return  $\text{true}$  if  $score > \text{thres}$ , else  $\text{false}$ 

```

number of positions $H = 1$.

F.1. Gumbel-max-based multibit watermarking

Recall the sequence-level score of text W for message M is derived as follows, where sk is the watermark key and u_t is the random value seeded by sk , and h context tokens from $W_{t-h:t}$,

$$\begin{aligned} S_M(W_t, \text{sk}) &= \ln \frac{1}{1 - \Psi(u_t, \psi(M))}, \\ C_M(W, \text{sk}) &= \frac{1}{T} \sum_{t=1}^T S_M(W_t, \text{sk}). \end{aligned} \quad (18)$$

Under the null hypothesis \mathcal{H}_0 , all C_M share the same non-watermarked distribution. Under the alternative hypothesis \mathcal{H}_1 , exactly one index M^* is “signal” while the remaining $2^m - 1$ are “null”, where M^* represents the message embedded by the encoder.

Under \mathcal{H}_0 , $\Psi \sim \text{Uniform}(0, 1)$ and hence $S_M(W_t, \text{sk}) \stackrel{d}{=} \text{Exp}(1)$. Therefore,

$$\begin{aligned} \mathbb{E}[C_M(W, \text{sk}) \mid \mathcal{H}_0] &= \mu_{\mathcal{H}_0} = 1, \\ \text{Var}(C_M(W, \text{sk}) \mid \mathcal{H}_0) &= \sigma_{\mathcal{H}_0}^2 = \frac{1}{T}. \end{aligned} \quad (19)$$

Under \mathcal{H}_1 , referring to equation (14) in (Fernandez et al., 2023), for the t -th watermarked token with bias $p_t \in (0, 1]$, $\Psi(u_t, \psi(M^*)) \sim \text{Beta}(\frac{1}{p_t}, 1)$ so that $1 - \Psi \sim \text{Beta}(1, \frac{1}{p_t})$. According to the digamma function ψ_0 and trigamma function ψ_1 defined in Lemma G.3,

$$\begin{aligned} \mathbb{E}[S_{M^*}(W_t, \text{sk})] &= \psi_0\left(1 + \frac{1}{p_t}\right) - \psi_0(1) := H_{1/p_t}, \\ \text{Var}(S_{M^*}(W_t, \text{sk})) &= \psi_1(1) - \psi_1\left(1 + \frac{1}{p_t}\right). \end{aligned} \quad (20)$$

Therefore, for the true message M^* ,

$$\begin{aligned} \mathbb{E}[C_{M^*} \mid \mathcal{H}_1] &= \mu_{\mathcal{H}_1} = \frac{1}{T} \sum_{t=1}^T H_{1/p_t}, \\ \text{Var}[C_{M^*} \mid \mathcal{H}_1] &= \sigma_{\mathcal{H}_1}^2 = \frac{1}{T^2} \sum_{t=1}^T [\psi_1(1) - \psi_1\left(1 + \frac{1}{p_t}\right)]. \end{aligned} \quad (21)$$

Let $Z = \max_{M \in \{0, \dots, 2^m - 1\}} \{C_M\}$. Since the sequence-level score $C_M(W, \text{sk})$ averages over T tokens, the Central Limit Theorem (CLT) suggests that, as T grows, $C_M(W, \text{sk}) \sim \mathcal{N}(\mu_{\mathcal{H}_0}, \sigma_{\mathcal{H}_0}^2)$. Besides, although the statistics $\{C_M\}$ are not strictly independent since they are calculated on the same text, each C_M is an average of T per-token scores with variance $O(1/T)$. As T grows, the variance of each C_M shrinks. Therefore, the event $\{Z > \tau\}$ is

potentially caused by one candidate C_M exhibiting an unusually large deviation, rather than by simultaneous moderate deviations of many correlated C_M . Hence, we can approximate $\{C_M\}$ as independent. By Lemma G.1, we obtain

$$\begin{aligned} \text{FPR}(\tau) &= \Pr(Z > \tau \mid \mathcal{H}_0) = 1 - \left[\Phi\left(\frac{\tau - \mu_{\mathcal{H}_0}}{\sigma_{\mathcal{H}_0}}\right) \right]^{2^m} \\ &\approx 2^m Q\left(\frac{\tau - \mu_{\mathcal{H}_0}}{\sigma_{\mathcal{H}_0}}\right), \end{aligned} \quad (22)$$

where as defined in Lemma G.1, $\Phi(\cdot)$ denotes the cumulative distribution function of the standard normal distribution while $Q(\cdot)$ is the gaussian tail probability.

Similarly, under \mathcal{H}_1 , we can approximate $C_{M^*}(W, \text{sk}) \sim \mathcal{N}(\mu_{\mathcal{H}_1}, \sigma_{\mathcal{H}_1}^2)$ and calculate FNR as

$$\begin{aligned} \text{FNR}(\tau) &= \Pr(Z < \tau \mid \mathcal{H}_1) = \Pr(C_{M^*} < \tau \mid \mathcal{H}_1) \\ &= \Phi\left(\frac{\tau - \mu_{\mathcal{H}_1}}{\sigma_{\mathcal{H}_1}}\right) = Q\left(\frac{\mu_{\mathcal{H}_1} - \tau}{\sigma_{\mathcal{H}_1}}\right), \end{aligned} \quad (23)$$

To solve the EER threshold, let $\text{FPR}(\tau^{\text{eer}}) = \text{FNR}(\tau^{\text{eer}})$. Let

$$\begin{aligned} z_0(\tau^{\text{eer}}) &= \frac{\tau^{\text{eer}} - \mu_{\mathcal{H}_0}}{\sigma_{\mathcal{H}_0}}, \\ z_1(\tau^{\text{eer}}) &= \frac{\mu_{\mathcal{H}_1} - \tau^{\text{eer}}}{\sigma_{\mathcal{H}_1}}, \end{aligned} \quad (24)$$

we write $z_0 = z_0(\tau^{\text{eer}})$ and $z_1 = z_1(\tau^{\text{eer}})$ for brevity, combining equation 22 and equation 23, then

$$z_1^2 = z_0^2 - 2m \ln 2 - 2 \ln\left(\frac{z_1}{z_0}\right). \quad (25)$$

Since z_0 and z_1 are of the same order as the EER operating points, $2 \ln\left(\frac{z_1}{z_0}\right)$ is lower-order. Thus, we obtain

$$z_1^2 \approx z_0^2 - 2m \ln 2. \quad (26)$$

Let $\Delta\mu = \mu_{\mathcal{H}_1} - \mu_{\mathcal{H}_0}$, and thus,

$$\sigma_0 z_0 + \sigma_1 z_1 = \Delta\mu \quad (27)$$

We first take $m = 0$. Therefore,

$$\tau_{m=0}^{\text{eer}} = \frac{\mu_{\mathcal{H}_0} \sigma_{\mathcal{H}_1} + \mu_{\mathcal{H}_1} \sigma_{\mathcal{H}_0}}{\sigma_{\mathcal{H}_0} + \sigma_{\mathcal{H}_1}} \quad (28)$$

Thus, plug equation 28 into equation 24, at $m = 0$,

$$z_0 = z_1 = z_{m=0} = \frac{\Delta\mu}{\sigma_{\mathcal{H}_0} + \sigma_{\mathcal{H}_1}}. \quad (29)$$

Now we take a first order perturbation for $m > 0$. Let

$$z_0 = z_{m=0} + \varepsilon_0, \quad z_1 = z_{m=0} + \varepsilon_1, \quad (30)$$

since $z_1^2 - z_0^2 = (z_{m=0} + \varepsilon_1)^2 - (z_{m=0} + \varepsilon_0)^2 \approx 2z(\varepsilon_1 - \varepsilon_0)$, from equation 26,

$$2z(\varepsilon_1 - \varepsilon_0) = -2m \ln 2. \quad (31)$$

Therefore,

$$\varepsilon_1 - \varepsilon_0 = -\frac{m \ln 2}{z_{m=0}} \quad (32)$$

Combining the identity $\mu_{\mathcal{H}_0} + \sigma_{\mathcal{H}_0} z_0 = \tau^{\text{eer}} = \mu_{\mathcal{H}_1} - \sigma_{\mathcal{H}_1} z_1$, we obtain

$$\sigma_{\mathcal{H}_0} \varepsilon_0 + \sigma_{\mathcal{H}_1} \varepsilon_1 = 0 \quad (33)$$

Furthermore, combining equation 29, equation 32 and equation 33, we obtain

$$\begin{aligned} \varepsilon_1 &= -\frac{\sigma_{\mathcal{H}_0}}{\Delta\mu} m \ln 2 \\ \varepsilon_0 &= \frac{\sigma_{\mathcal{H}_1}}{\Delta\mu} m \ln 2. \end{aligned} \quad (34)$$

Therefore, from equation 30, we obtain

$$z_1 \approx z_{m=0} - \frac{\sigma_{\mathcal{H}_0}}{\Delta\mu} m \ln 2 \quad (35)$$

Substituting equation 29 gives the EER approximation

$$\text{EER}_{\text{Gumbel}} \approx Q \left(\frac{\Delta\mu}{\sigma_{\mathcal{H}_0} + \sigma_{\mathcal{H}_1}} - \frac{\sigma_{\mathcal{H}_0}}{\Delta\mu} m \ln 2 \right). \quad (36)$$

For clarity, suppose that all tokens share the same bias $p_t \equiv p$. Then

$$\begin{aligned} \mu_{\mathcal{H}_1} &= H_{1/p}, \\ \sigma_{\mathcal{H}_1}^2 &= \frac{\psi_1(1) - \psi_1(1 + 1/p)}{T}, \\ \Delta\mu &= H_{1/p} - 1. \end{aligned} \quad (37)$$

Plugging these into equation 36, therefore,

$$\begin{aligned} \text{EER}_{\text{Gumbel}} &\approx \\ Q \left(\frac{(H_{1/p} - 1)\sqrt{T}}{1 + \sqrt{\psi_1(1) - \psi_1(1 + 1/p)}} - \frac{m \ln 2}{(H_{1/p} - 1)\sqrt{T}} \right). \end{aligned} \quad (38)$$

Relating p to the vocabulary size. In Gumbel-max sampling for an LLM with the vocabulary size of V , suppose κV candidates enter a uniform competition, which means each candidate receives an i.i.d. PRF value $U \sim \text{Uniform}(0, 1)$ and the winner achieves $U_{(\kappa V)} = \max\{U_1, \dots, U_{\kappa V}\} \sim \text{Beta}(\kappa V, 1)$. Intuitively, κ increases with the entropy. Therefore, we can identify an effective pool size $\kappa V \simeq 1/p$. Equivalently, κ can be characterized via the entropy of the next-token distribution. Let $p_t(\cdot) = p_{\text{LM}}(\cdot \mid x_{<t})$ denote the next-token probability distribution at step t , and define

$$H(p_t) \triangleq -\sum_{i=1}^V p_t(i) \log p_t(i). \quad (39)$$

The effective number of competing tokens is then given by $\exp(H(p_t))$, which corresponds to the size of a uniform distribution with the same uncertainty. Accordingly, we have $\kappa \approx \exp(H(p_t))/V$. Furthermore, we set $\frac{1}{p} = \kappa V = \exp(H(p_t))$ as estimated in a development set.

Denoting $\mathcal{H} = H(p_t)$ and substituting $\frac{1}{p} = \exp(\mathcal{H})$ into equation 38 gives

$$\begin{aligned} \text{EER}_{\text{Gumbel}} &\approx \\ Q \left(\frac{(H_{\exp(\mathcal{H})} - 1)\sqrt{T}}{1 + \sqrt{\psi_1(1) - \psi_1(1 + \exp(\mathcal{H}))}} - \frac{m \ln 2}{(H_{\exp(\mathcal{H})} - 1)\sqrt{T}} \right). \end{aligned} \quad (40)$$

For large V , using the expansions in Lemma G.3, we have

$$\begin{aligned} H_{\exp(\mathcal{H})} &= \ln(\exp(\mathcal{H})) + \gamma = \mathcal{H} + \gamma, \\ \psi_1(1) - \psi_1(1 + \exp(\mathcal{H})) &= \frac{\pi^2}{6}, \end{aligned} \quad (41)$$

where γ is Euler's constant defined in Lemma G.3. Substituting these expansions into equation 40, we obtain

$$\text{EER}_{\text{Gumbel}} \approx Q(z_{\mathcal{H}}), \quad (42)$$

where

$$z_{\mathcal{H}} = \frac{(\mathcal{H} + \gamma - 1)\sqrt{T}}{1 + \pi/\sqrt{6}} - \frac{m \ln 2}{(\mathcal{H} + \gamma - 1)\sqrt{T}}. \quad (43)$$

For large $z_{\mathcal{H}}$, we approximate

$$\begin{aligned} \log \text{EER}_{\text{Gumbel}} &= -\frac{z_{\mathcal{H}}^2}{2} - \log(z_{\mathcal{H}}\sqrt{2\pi}) \\ &= -c_1 T(\mathcal{H} + \gamma - 1)^2 + \\ &\quad c_2 m - \frac{(m \ln 2)^2}{2T(\mathcal{H} + \gamma - 1)^2} - \log(z_{\mathcal{H}}\sqrt{2\pi}), \end{aligned} \quad (44)$$

where the constants $c_1 = \frac{1}{2(1+\pi/\sqrt{6})^2}$ and $c_2 = \frac{\ln 2}{1+\pi/\sqrt{6}}$.

The dominant term in equation 44 scales quadratically with \mathcal{H} , while the dependence on the symbol size m appears as a linear correction in the exponent. The remaining terms are strictly lower order in \mathcal{H} . Consequently, for fixed m and sufficiently large \mathcal{H} ,

$$\log \text{EER}_{\text{Gumbel}} = -c_1 T \mathcal{H}^2 + c_2 m + o(T \mathcal{H}^2), \quad (45)$$

which implies an exponential decay of $\text{EER}_{\text{Gumbel}}$ at a quadratic rate in \mathcal{H} . Furthermore, increasing the symbol size m leads to a larger EER through a linear shift in the exponent.

F.2. Tournament sampling based multi-bit watermarking

Recall in equation 4 the score of t -th token for message M

$$S_M(\text{sk}, W_t) = \frac{1}{L} \sum_{\ell=1}^L \alpha_\ell \Psi(u_{t,\ell}, \psi(M)), \quad (46)$$

and the sequence-level statistic for message M as the per-token average

$$C_M(\text{sk}, W) = \frac{1}{T} \sum_{t=1}^T S_M(\text{sk}, W_t). \quad (47)$$

In this derivation, we treat $m = 1$, where the construction enforces $S_0(\text{sk}, W_t) + S_1(\text{sk}, W_t) \equiv 1$ per token from the property of mirroring. Define

$$\begin{aligned} Z_t &= \max\{S_0(\text{sk}, W_t), S_1(\text{sk}, W_t)\} \\ &= \frac{1}{2} + \left| S_0(\text{sk}, W_t) - \frac{1}{2} \right|, \end{aligned} \quad (48)$$

and detect with $C_{\max} = \frac{1}{T} \sum_{t=1}^T Z_t$. For easier analysis, we assume $\frac{1}{L} \sum_{\ell=1}^L \alpha_\ell = 1$.

Under null hypothesis, at each layer ℓ , $\Psi \sim \text{Uniform}(0, 1)$, hence

$$\begin{aligned} \mathbb{E}[S_0(\text{sk}, W_t) \mid \mathcal{H}_0] &= \frac{1}{L} \sum_{\ell=1}^L \frac{\alpha_\ell}{2} = \frac{1}{2}, \\ \text{Var}[S_0(\text{sk}, W_t) \mid \mathcal{H}_0] &= \frac{1}{L^2} \sum_{\ell=1}^L \alpha_\ell^2 \text{Var}(\Psi) = \frac{A}{12L^2}, \end{aligned} \quad (49)$$

where $A = \sum_{\ell=1}^L \alpha_\ell^2$. Approximating $S_0(\text{sk}, W_t) - \frac{1}{2}$ by $\mathcal{N}(0, \frac{A}{12L^2})$ and using the Lemma G.2,

$$\begin{aligned} \mathbb{E} \left| S_0(\text{sk}, W_t) - \frac{1}{2} \right| &= \sqrt{\frac{A}{6\pi L^2}}, \\ \text{Var} \left| S_0(\text{sk}, W_t) - \frac{1}{2} \right| &= \frac{A}{12L^2} \left(1 - \frac{2}{\pi} \right). \end{aligned} \quad (50)$$

Therefore

$$\begin{aligned} \mathbb{E}[Z_t \mid \mathcal{H}_0] &= \frac{1}{2} + \sqrt{\frac{A}{6\pi L^2}}, \\ \text{Var}[Z_t \mid \mathcal{H}_0] &= \frac{A}{12L^2} \left(1 - \frac{2}{\pi} \right), \end{aligned} \quad (51)$$

By central limit theorem (CLT), for $C_{\max} = \frac{1}{T} \sum_t Z_t$,

$$\begin{aligned} \mu_{\mathcal{H}_0} &= \mathbb{E}[C_{\max} \mid \mathcal{H}_0] = \frac{1}{2} + \sqrt{\frac{A}{6\pi L^2}}, \\ \sigma_{\mathcal{H}_0}^2 &= \text{Var}[C_{\max} \mid \mathcal{H}_0] = \frac{A}{12L^2 T} \left(1 - \frac{2}{\pi} \right). \end{aligned} \quad (52)$$

We can derive the FPR as

$$\text{FPR} = \Pr[C_{\max} > \tau \mid \mathcal{H}_0] = Q\left(\frac{\tau - \mu_{\mathcal{H}_0}}{\sigma_{\mathcal{H}_0}}\right) \quad (53)$$

On the other hand, under the alternative hypothesis \mathcal{H}_1 , at layer ℓ , refer to Corollary 28 in SynthID (Dathathri et al., 2024), the mirrored random variable described by the cumulative density function (CDF) and probability density function (PDF) as follows,

$$\begin{aligned} F_{\Psi_\ell}(x) &= C_{wm}^\ell x + (1 - C_{wm}^\ell)x^2, \\ f_{\Psi_\ell}(x) &= C_{wm}^\ell + 2(1 - C_{wm}^\ell)x, \end{aligned} \quad (54)$$

where $C_{wm}^\ell \in [0, 1]$ represents the collision probability at layer ℓ as defined in Definition 22 in SynthID, which is the probability that two samples drawn i.i.d. from the probability distribution of tokens at layer ℓ are the same. Hence,

$$\begin{aligned} \mathbb{E}[\Psi_\ell] &= \frac{2}{3} - \frac{C_{wm}^\ell}{6}, \\ \text{Var}(\Psi_\ell) &= \frac{2 + 2C_{wm}^\ell - (C_{wm}^\ell)^2}{36}. \end{aligned} \quad (55)$$

Hence the per-token $S_0(t) = \frac{1}{L} \sum_\ell \alpha_\ell \Psi_\ell$ has

$$\begin{aligned} \mu_S &= \mathbb{E}[S_0(\text{sk}, W_t) \mid \mathcal{H}_1] = \frac{1}{L} \sum_{\ell=1}^L \alpha_\ell \left(\frac{2}{3} - \frac{C_{wm}^\ell}{6} \right), \\ v_S &= \text{Var}[S_0(\text{sk}, W_t) \mid \mathcal{H}_1] \\ &= \frac{1}{L^2} \sum_{\ell=1}^L \alpha_\ell^2 \frac{2 + 2C_{wm}^\ell - (C_{wm}^\ell)^2}{36}. \end{aligned} \quad (56)$$

Let $\mu_\Delta = \mu_S - \frac{1}{2}$. Using the Lemma G.2 again,

$$\begin{aligned} \mathbb{E}|S_0(\mathbf{sk}, W_t) - \frac{1}{2}| &= \sqrt{\frac{2}{\pi}} \sqrt{v_S} \exp\left(-\frac{\mu_\Delta^2}{2v_S}\right) + \mu_\Delta \left[1 - 2\Phi\left(-\frac{\mu_\Delta}{\sqrt{v_S}}\right)\right] \\ &=: \text{FNmean}(\mu_\Delta, v_S), \\ \text{Var}(|S_0(\mathbf{sk}, W_t) - \frac{1}{2}|) &= \mu_\Delta^2 + v_S - (\mathbb{E}|S_0(\mathbf{sk}, W_t) - \frac{1}{2}|)^2 \\ &=: \text{FNvar}(\mu_\Delta, v_S). \end{aligned} \quad (57)$$

Thus for $Z_t = \frac{1}{2} + |S_0(\mathbf{sk}, W_t) - \frac{1}{2}|$,

$$\mathbb{E}[Z_t | \mathcal{H}_1] = \frac{1}{2} + \text{FNmean}(\mu_\Delta, v_S), \quad (58)$$

$$\text{Var}[Z_t | \mathcal{H}_1] = \text{FNvar}(\mu_\Delta, v_S),$$

and

$$\begin{aligned} \mu_{\mathcal{H}_1} &= \mathbb{E}[C_{\max} | \mathcal{H}_1] = \mathbb{E}[Z_t | \mathcal{H}_1], \\ \sigma_{\mathcal{H}_1}^2 &= \text{Var}[C_{\max} | \mathcal{H}_1] = \text{Var}[Z_t | \mathcal{H}_1]/T. \end{aligned} \quad (59)$$

We can derive the FNR as

$$\text{FNR} = \Pr[C_{\max} < \tau | H_1] = \Phi\left(\frac{\tau - \mu_{\mathcal{H}_1}}{\sigma_{\mathcal{H}_1}}\right) \quad (60)$$

Combining equation 53 and equation 60, let FPR = FNR, we can derive the EER is

$$\begin{aligned} \text{EER}_{\text{tour}} &= \text{FPR}(\tau^{\text{eer}}) = \text{FNR}(\tau^{\text{eer}}) \\ &= Q\left(\frac{\mu_{\mathcal{H}_1} - \mu_{\mathcal{H}_0}}{\sigma_{\mathcal{H}_0} + \sigma_{\mathcal{H}_1}}\right). \end{aligned} \quad (61)$$

For easier analysis, we assume $\frac{1}{L} \sum_{\ell=1}^L \alpha_\ell = 1$, define

$$\begin{aligned} C_1 &:= \frac{1}{L} \sum_{\ell=1}^L \alpha_\ell C_{wm}^\ell, \\ C_2 &:= \frac{1}{L} \sum_{\ell=1}^L \alpha_\ell^2 \frac{2 + 2C_{wm}^\ell - (C_{wm}^\ell)^2}{36}. \end{aligned} \quad (62)$$

Therefore,

$$\begin{aligned} \mu_\Delta &= \frac{1 - C_1}{6}, \\ v_S &= \frac{C_2}{L}. \end{aligned} \quad (63)$$

Let $z = \frac{\mu_\Delta}{\sqrt{v_S}}$, which means z depends on C_1, C_2 , and L . Then the folded-normal mean in equation 57 satisfies

$$\text{FNmean}(\mu_\Delta, v_S) = \mu_\Delta \left(\sqrt{\frac{2}{\pi}} \frac{e^{-z^2/2}}{z} + 2\Phi(z) - 1 \right). \quad (64)$$

Let $m(z) = \sqrt{\frac{2}{\pi}} \frac{e^{-z^2/2}}{z} + 2\Phi(z) - 1$. Therefore, $\text{FNmean}(\mu_\Delta, v_S) = \mu_\Delta m(z)$. Hence,

$$\mu_{\mathcal{H}_1} = \frac{1}{2} + \mu_\Delta m(z). \quad (65)$$

Meanwhile,

$$\begin{aligned} \sigma_{\mathcal{H}_1} &= \sqrt{\frac{\mu_\Delta^2 + v_S - (\text{FNmean}(\mu_\Delta, v_S))^2}{T}} \\ &= \frac{1}{\sqrt{T}} \sqrt{\mu_\Delta^2 \left(1 - m^2(z) + \frac{1}{z^2}\right)}. \end{aligned} \quad (66)$$

Let

$$\kappa_0 = \sqrt{\frac{A}{6\pi L^2}}, \quad (67)$$

$$\kappa_1 = \sqrt{\frac{A(1 - \frac{2}{\pi})}{12L^2}}, \quad (68)$$

$$\kappa_2 = \mu_\Delta m(z), \quad (69)$$

and

$$\kappa_3 = \mu_\Delta \sqrt{1 - m^2(z) + \frac{1}{z^2}}, \quad (70)$$

then

Hence, by equation 61,

$$\begin{aligned} \text{EER}_{\text{tour}} &= Q\left(\frac{\mu_{\mathcal{H}_1} - \mu_{\mathcal{H}_0}}{\sigma_{\mathcal{H}_0} + \sigma_{\mathcal{H}_1}}\right) \\ &= Q\left(\frac{\kappa_2 - \kappa_0}{\kappa_3 + \kappa_1} \sqrt{T}\right). \end{aligned} \quad (71)$$

Define

$$\begin{aligned} \Gamma &= \Gamma(C_1, C_2, L) = \frac{\kappa_2}{\kappa_3 + \kappa_1}, \\ \beta &= \beta(C_1, C_2, L) = \frac{\kappa_0}{\kappa_3 + \kappa_1}, \end{aligned} \quad (72)$$

Then

$$\text{EER}_{\text{tour}} = Q\left((\Gamma - \beta)\sqrt{T}\right). \quad (73)$$

Using Lemma G.1, we obtain

$$\text{EER}_{\text{tour}} \approx \frac{\exp\left(-\frac{T}{2}(\Gamma - \beta)^2\right)}{\sqrt{2\pi T}(\Gamma - \beta)}. \quad (74)$$

Taking the logarithm of equation 74 yields

$$\log \text{EER}_{\text{tour}} = -\frac{T}{2}(\Gamma - \beta)^2 - \frac{1}{2} \log 2\pi T - \log(\Gamma - \beta). \quad (75)$$

Since equation 62 shows that both C_1 and C_2 depend on the layer-wise collision probabilities $\{C_{\ell, \text{wm}}\}_{\ell=1}^L$, we define

$$\zeta(L, C_{1, \text{wm}}, \dots, C_{L, \text{wm}}) \triangleq \Gamma(C_1, C_2, L) - \beta(C_1, C_2, L). \quad (76)$$

For notational convenience, we denote the collection of collision-related parameters by

$$\mathbf{c} \triangleq (L, C_{1, \text{wm}}, C_{2, \text{wm}}, \dots, C_{L, \text{wm}}). \quad (77)$$

Hence,

$$\log \text{EER}_{\text{tour}} = -\frac{T}{2}\zeta^2(c) - \frac{1}{2} \log 2\pi T - \log \zeta(c). \quad (78)$$

G. Lemmas

Lemma G.1 Let $X_1, \dots, X_K \stackrel{\text{i.i.d.}}{\sim} \mathcal{N}(0, 1)$ and $G_K = \max_i X_i$. For large z ,

$$\Pr(G_K > z) = 1 - (1 - Q(z))^K = K Q(z) (1 + o(1)), \quad (79)$$

where $\Phi(z)$ denotes the cumulative distribution function of the standard normal distribution⁴ and $Q(z) = 1 - \Phi(z)$ is its Gaussian tail probability.

Lemma G.2 Let $X \sim \mathcal{N}(\mu, \sigma^2)$ and $Y = |X|$. Then

$$\mathbb{E}[Y] = \sigma \sqrt{\frac{2}{\pi}} \exp\left(-\frac{\mu^2}{2\sigma^2}\right) + \mu [1 - 2\Phi(-\frac{\mu}{\sigma})], \quad (80)$$

and

$$\text{Var}(Y) = \mu^2 + \sigma^2 - (\mathbb{E}[Y])^2. \quad (81)$$

Lemma G.3 Let $T \sim \text{Beta}(a, b)$. Then

$$\begin{aligned} \mathbb{E}[\ln T] &= \psi_0(a) - \psi_0(a + b), \\ \text{Var}(\ln T) &= \psi_1(a) - \psi_1(a + b), \end{aligned} \quad (82)$$

where the digamma function $\psi_0(x)$ for $x > 0$ is defined as

$$\psi_0(x) = -\gamma + \sum_{n=0}^{\infty} \left(\frac{1}{n+1} - \frac{1}{n+x} \right), \quad (83)$$

with γ the Euler's constant. The trigamma function $\psi_1(x)$ for $x > 0$ is defined as

$$\psi_1(x) = \sum_{n=0}^{\infty} \frac{1}{(n+x)^2}. \quad (84)$$

⁴https://en.wikipedia.org/wiki/Normal_distribution

In particular, for $x > 0$, let the generalized harmonic number $H_x = \psi_0(x+1) - \psi_0(1)$. As $x \rightarrow \infty$,

$$H_x = \ln x + \gamma. \quad (85)$$

H. Experimental Setup

Unless otherwise specified, all experiments use the Llama-2-7B model (Touvron et al., 2023) on a text completion task. We construct prompts from the RealNewsLike subset of C4 (Raffel et al., 2020). We randomly select 500 documents, truncate each document to obtain a prefix, and ask the model to generate a continuation conditioned on that prefix. Most results in the main paper are reported on this setting. To assess the generality of MirrorMark beyond this model and task, we additionally evaluate on the Gemma-7B-it (Team et al., 2024) model on an instruction-following task. We randomly sample 500 prompts from the ELI5 dataset (Fan et al., 2019), treat them as user instructions, and generate model responses.

Following (Dathathri et al., 2024), we use top-100 sampling with temperature of 1.0 for all evaluated watermarking approaches. For CABS, we use the same hyperparameters throughout the experiments, where $h = 4$, $f = 3$, $W = 4$, and $\text{max_len} = \text{max_factor} \cdot H$ with $\text{max_factor} = 1.5$ and H denoting the number of positions in the context. Following (Dathathri et al., 2024), our experiments use a default of 30 tournament layers. For each combination of m and base model in tournament-sampling-based MirrorMark, we train a separate Bayesian detector using 10,000 watermarked samples and 10,000 non-watermarked samples generated for that specific value of m . We randomly split the watermarked and non-watermarked feature files into an 80% training set and a 20% validation set. The detector is trained with the Adam optimizer using a learning rate of 3×10^{-3} , a batch size of 64, and up to 100 epochs. We select the model that achieves the highest validation TPR at 1% FPR, and report its performance in the main paper.

For all baseline comparisons, we follow the default symbol sizes m specified in the original papers, as these settings are reported to yield their best performance. In particular, MPAC uses $m = 2$, StealthInk uses $m = 1$, and RSBH uses $m = 6$. Therefore, to embed b bits, $H = \frac{b}{m}$ positions are needed.

I. Additional Results

I.1. Comparison with Gumbel-max-based multi-bit extension ThreeBricks (Fernandez et al., 2023)

We compare our Gumbel-max-based MirrorMark with the multi-bit extension proposed by ThreeBricks (Fernandez et al., 2023), which also builds upon Gumbel-max zero-bit watermarking. As shown in Fig. 5, across different m , ThreeBricks consistently underperforms MirrorMark in terms of bit accuracy. This performance gap arises from a fundamental design difference. ThreeBricks formulates multi-bit decoding as a multi-class hypothesis testing problem via cyclic shifts of a shared random source, where each token contributes evidence across all message hypotheses and incurs a multiple-testing penalty as the message space grows. In contrast, MirrorMark employs a single-key structured mirroring construction that decomposes multi-bit decoding into a set of complementary binary contrasts, explicitly maximizing hypothesis separation at the per-token level. As a result, MirrorMark achieves stronger statistical efficiency and higher bit accuracy under the same token budget.

I.2. Performance comparison over 200 and 400 tokens

We present the performance comparison across different approaches over 200 and 400 tokens, respectively as in Table 4 and Table 5, where the watermarked text generated by each approach is embedded with 36 bits and 54 bits, respectively.

I.3. Repetition score and LLM-as-judge score of the text generated with watermarking scheme

We further evaluate the linguistic quality of MirrorMark using two complementary metrics: (1) an LLM-as-a-judge assessment with GPT-4o as in Fig. 6, and (2) a repetition-based analysis using distinct-2 and repetition rate as in Table 6.

For the LLM-as-a-judge study, GPT-4o scored each text along four dimensions: coherence, clarity, naturalness, and overall quality. Following (Jovanović et al., 2024), we design the following GPT4o Judge prompt explicitly to ignore truncation effects and focus solely on linguistic fluency.

Across all configurations, MirrorMark achieves GPT-4o scores that are statistically indistinguishable from the non-watermarked baseline. The overall score difference consistently stays within 0.05–0.10, well inside the natural variance of GPT-4o evaluations. These results confirm that mod-1 mirroring does not degrade linguistic quality, aligning with our theoretical guarantee that MirrorMark is distribution-preserving. In contrast, distortion-based baselines such as MPAC and RSBH exhibit noticeably lower GPT-4o scores, consistent with their higher perplexity and the known side effects of their logit-biasing mechanisms.

The diversity analysis further reinforces these findings. Although MPAC and RSBH report high distinct-2 and low repetition rates, this behavior is driven by artificially skewing the token distribution away from natural language usage, which corresponds to their lower GPT-4o scores. In comparison, MirrorMark, especially the tournament-sampling variant, achieves distinct-2 and repetition rates nearly identical to non-watermarked text, demonstrating that it preserves natural linguistic diversity. While Gumbel-max is inherently more deterministic under top- k sampling and thus yields slightly lower diversity, GPT-4o evaluations confirm that this does not harm fluency or naturalness, as the generated sentences remain coherent and well-structured.

GPT-4o Judge Prompt

You are an impartial expert evaluator of linguistic text quality.

The given text is a continuation generated from a truncated C4 sample (15–20 words). The text may start or end abruptly because the generation length is fixed (e.g., 300 tokens). Do **NOT** penalize truncation or incompleteness.

Evaluate **ONLY** linguistic quality:

- Coherence — logical flow of ideas
- Clarity — easy to understand
- Naturalness — how fluent / human-written the text appears

Rate each from 1 to 5. Compute “overall” as the average of the three.

Return only a JSON object in exactly the following structure:

```
{
  "coherence": float,
  "clarity": float,
  "naturalness": float,
  "overall": float
}
```

Text: <<<TEXT>>>

I.4. Performance of MirrorMark in 72 Bits and 90 Bits

Fig. 7 demonstrates the AUC of MirrorMark in 72 bits and 90 bits across varying number of tokens, respectively.

I.5. Cross-language adaptation

To evaluate whether MirrorMark is tied to a specific language or can be reliably applied across languages, we conduct a cross-language experiment using the multilingual XL-Sum dataset (Hasan et al., 2021) on Gemma-7Bit (Team et al., 2024). For each language (English, Chinese, and Russian), we sample summaries from XL-Sum and prompt the model to generate full news articles in the cor-

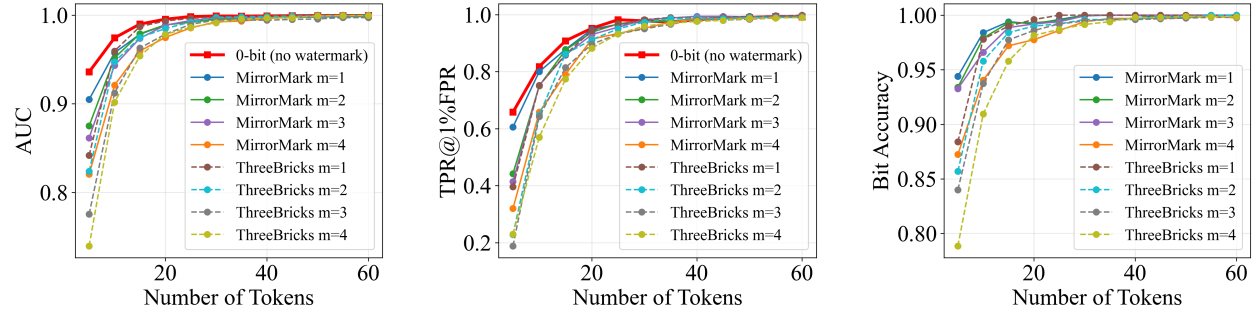

 Figure 5: Performance comparison between Gumbel-max-based MirrorMark and ThreeBricks, $H = 1$.

Table 4: Mean perplexity and detectability for different approaches on 200 tokens. Each perplexity is given with a 90% confidence interval based on bootstrapping.

Method	36 Bits				54 Bits			
	AUC	TPR@1%FPR	Bit Acc.	Perplexity	AUC	TPR@1%FPR	Bit Acc.	Perplexity
Non Watermark	—	—	—	7.7836 [7.6024, 7.9665]	—	—	—	7.7836 [7.6024, 7.9665]
MPAC	0.9903	0.9400	0.8893	9.8604 [9.6782, 10.0450]	0.9913	0.9180	0.8394	10.1388 [9.9353, 10.3464]
RSBH	0.9983	0.9980	0.9992	32.6466 [31.2956, 34.0539]	0.9979	0.9980	0.9928	32.6994 [31.2430, 34.2013]
StealthInk	0.9787	0.6540	0.8423	7.3038 [7.0626, 7.5421]	0.9654	0.4420	0.7896	7.2339 [6.9976, 7.4662]
Gumbel-max	1.0	0.9980	0.9613	7.5709 [7.3951, 7.7503]	0.9998	0.9960	0.9338	7.6708 [7.4902, 7.8644]
Tour-Wmean	0.9955	0.9880	0.9345	7.7710 [7.6014, 7.9373]	0.9999	0.9980	0.8962	7.7592 [7.5870, 7.9293]
Tour-Bayes	0.9954	0.9860	0.9495	7.7710 [7.6014, 7.9373]	0.9992	0.9800	0.9051	7.7592 [7.5870, 7.9293]

Table 5: Mean perplexity and detectability for different approaches on 400 tokens. Each perplexity is given with a 90% confidence interval based on bootstrapping.

Method	36 Bits				54 Bits			
	AUC	TPR@1%FPR	Bit Acc.	Perplexity	AUC	TPR@1%FPR	Bit Acc.	Perplexity
Non Watermark	—	—	—	7.0513 [6.9156, 7.1849]	—	—	—	7.0513 [6.9156, 7.1849]
MPAC	0.9970	0.9820	0.9599	8.8160 [8.6754, 8.9583]	0.9960	0.9940	0.9227	8.8811 [8.7232, 9.0393]
RSBH	0.9999	1.0	1.0	32.5108 [32.1111, 34.9533]	0.9990	1.0	0.9972	33.6699 [32.1541, 35.2284]
StealthInk	0.9941	0.9500	0.9204	6.5826 [6.4060, 6.7593]	0.9952	0.9400	0.8748	6.5893 [6.4053, 6.7813]
Gumbel-max	1.0	1.0	0.9929	6.8081 [6.6618, 6.9545]	1.0	1.0	0.9849	6.8855 [6.7453, 7.0332]
Tour-Wmean	0.9998	0.9960	0.9811	7.1759 [7.0406, 7.3120]	1.0	1.0	0.9665	7.0888 [6.9534, 7.2243]
Tour-Bayes	0.9996	0.9920	0.9819	7.1759 [7.0406, 7.3120]	0.9997	0.9960	0.9706	7.0888 [6.9534, 7.2243]

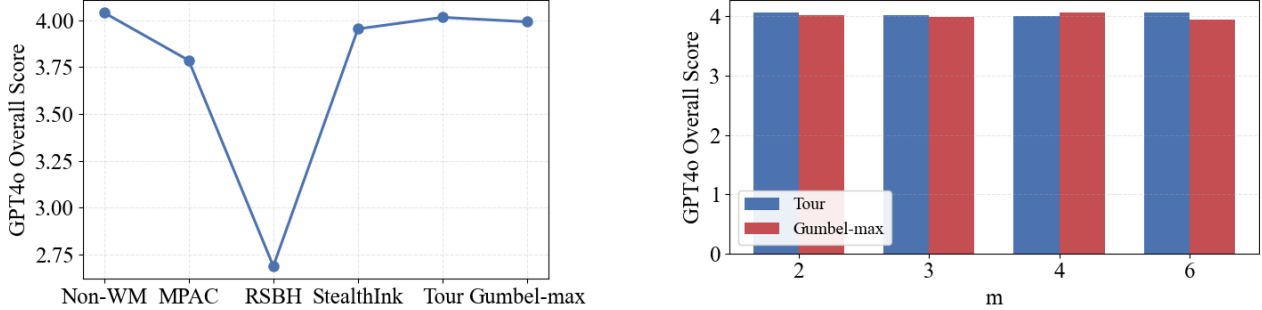

 Figure 6: Text quality scored by GPT4o over 300 tokens, where $m = 3$ and $H = 12$

Table 6: Text quality scored with distinct-2 and repetition rate across watermarking schemes, 36 bits are embedded in 300 tokens.

	Non-watermarked	MPAC	RSBH	StealthInk	TB (m=2)	TB (m=3)	TB (m=4)	TB (m=6)	G-max (m=2)	G-max (m=3)	G-max (m=4)	G-max (m=6)
Distinct-2	0.9471	0.9624	0.9648	0.9498	0.9452	0.9494	0.9475	0.9451	0.9277	0.9269	0.9209	0.9292
Repetition Rate	0.4542	0.4183	0.3528	0.4410	0.4538	0.4504	0.4509	0.4561	0.4733	0.4761	0.4849	0.4752

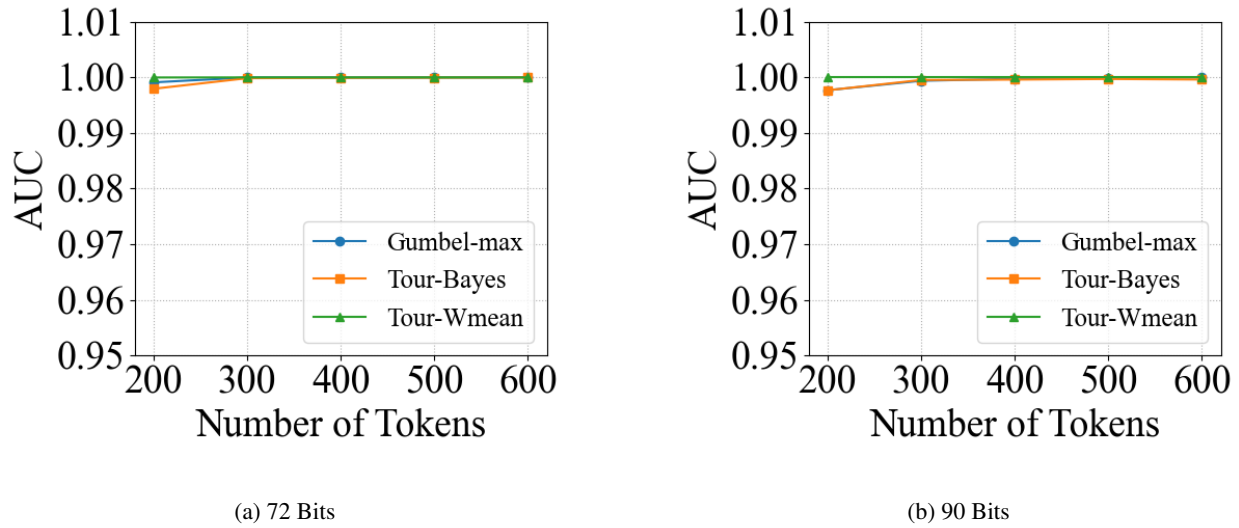


Figure 7: AUC of MirrorMark across varying number of tokens respectively with 72 and 90 bits embedded.

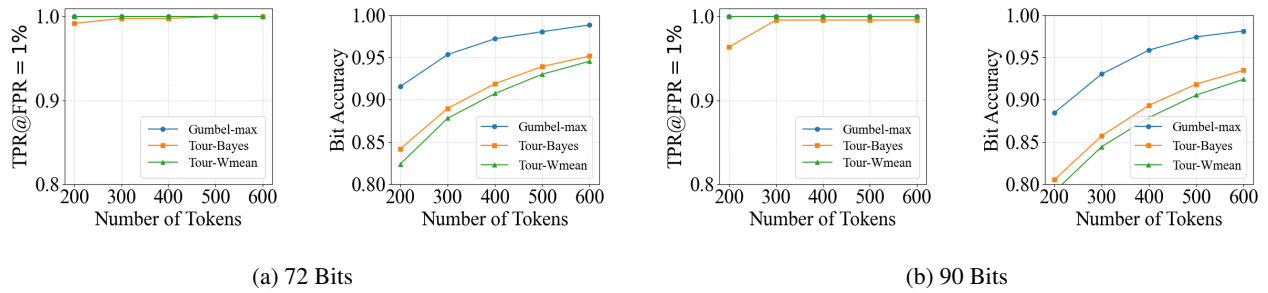


Figure 8: Detectability of MirrorMark across varying number of tokens repectively with 72 and 90 bits embedded.

responding language. During generation, we apply exactly the same MirrorMark watermarking rule as in our main experiments. For each language, we generate 500 paired watermarked and non-watermarked samples of length 200 tokens, and evaluate both the Bayesian detector for tournament sampling (Tour-Bayes) and the analytic detector for Gumbel-max.

Figure 9 shows that a detection threshold τ calibrated in one language does not perfectly transfer to another. In particular, when a threshold learned on English is applied to Chinese, the empirical false positive rate (FPR) on Chinese increases, whereas applying the same threshold to Russian yields largely unchanged behavior. Conversely, a threshold calibrated on Chinese becomes overly conservative when applied to English or Russian, reducing both FPR and true positive rate (TPR).

This cross-language threshold mismatch is consistent with a well-established empirical observation (Montemurro & Zanette, 2011): Chinese text exhibits systematically lower next-token entropy than English and Russian, while English and Russian have similar entropy profiles. As a result, both watermarked and non-watermarked scores for Chinese are expected to be shifted toward larger values, even when the separation between the two hypotheses remains comparable. Consequently, a threshold τ calibrated on English (where the non-watermarked distribution is farther left) becomes slightly too permissive for Chinese, increasing FPR, whereas a threshold calibrated on Chinese becomes too strict when applied to English or Russian.

Overall, Fig. 9 demonstrates that MirrorMark is not tied to English or any particular dataset. Across all three languages, both the tournament-based (Tour-Bayes) and Gumbel-max variants remain reliably detectable, with similar ROC trends. The observed differences are limited to small score-scale shifts induced by language-specific entropy characteristics, which can be addressed through simple threshold recalibration. These results support our claim that MirrorMark is a data-agnostic generative watermark whose detectability is primarily governed by sequence length and entropy, rather than by language or domain.

1.6. Detectability and text quality on instruction task

Fig. 10 and Fig. 11 report the detectability of MirrorMark on instruction-following generation, where 500 randomly selected ELI5 prompts (Fan et al., 2019) are evaluated using the Gemma-7B-it model (Team et al., 2024), where the temperature is 1.0.

We first present the empirical EER results in Fig. 10. We observe that Tour-Bayes yields lower EER than Tour-Wmean under the same configuration. This suggests that,

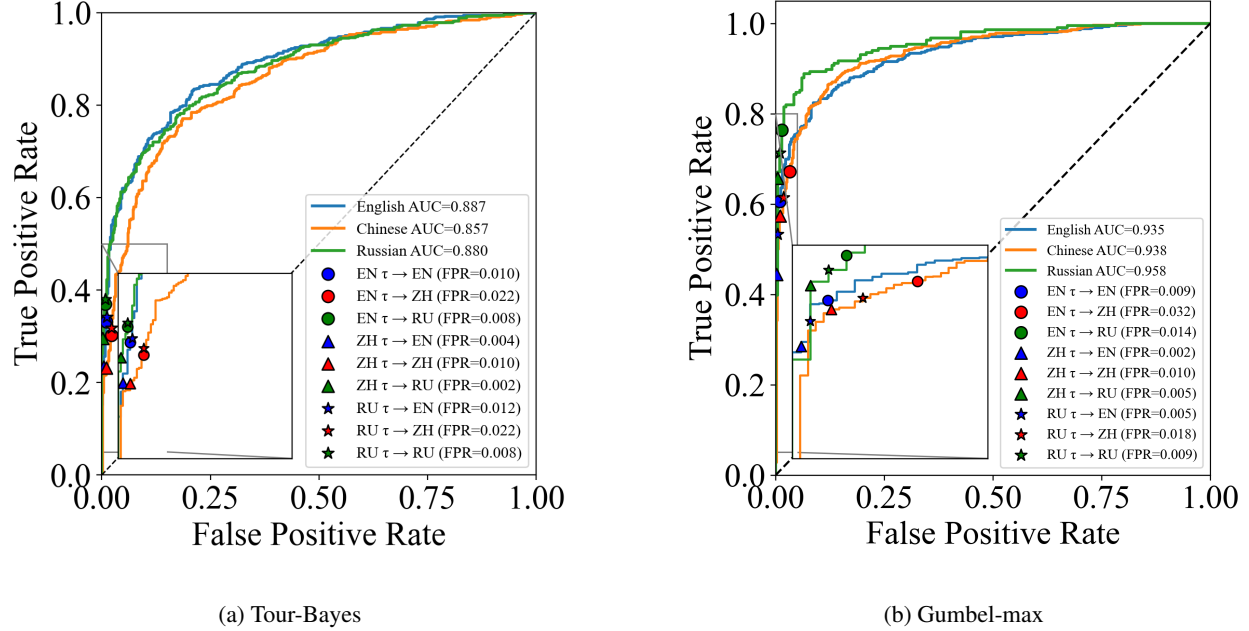
when entropy is constrained, a more structured aggregation rule instead of a fixed and layer-dependent weighting scheme, can be more robust to the limited and highly correlated u -value evidence accumulated across layers. In addition, replacing Uniform(0, 1) with Bernoulli-distributed u values further reduces EER in this low-entropy regime. This behavior is consistent with the intuition that, under constrained decoding, more extreme random variables better preserve per-step contrast and are less susceptible to collision effects, whereas Uniform(0, 1) samples tend to concentrate in a narrow mid-range and accumulate weaker evidence across layers. We emphasize that this Bernoulli variant is introduced purely as an ablation to isolate the role of the u -value distribution: because Bernoulli u values are inherently binary, it can embed at most one bit and therefore does not extend to the multi-bit setting considered throughout the paper.

Fig. 11 then reports practical detection metrics, including TPR@1%FPR, AUC, and bit accuracy. Here we include Tour-Bayes as a representative tournament-based detector under the main evaluation protocol. We observe that Gumbel-max-based MirrorMark achieves higher detection performance than tournament-based MirrorMark across all metrics. For example, in Fig. 11(b), the Gumbel-max-based MirrorMark reaches approximately 80% TPR@1%FPR at 100 tokens, while in Fig. 11(e), the tournament-based MirrorMark reaches around 65% at the same length.

Despite the reduced detectability, MirrorMark maintains text quality comparable to non-watermarked text. Table 7 reports the perplexity of 200-token instruction-following responses. Across all watermarking configurations, the perplexity of watermarked text remains very close to the non-watermarked baseline, and the 90% confidence intervals largely overlap. Switching the tournament sampler from Uniform(0, 1) to Bernoulli $u \in \{0, 1\}$ slightly increases perplexity to 1.8208 ([1.7882, 1.8541]) for $m=1$, but the change remains modest and does not indicate systematic degradation in output quality.

1.7. Detectability Comparison over different m for MirrorMark after copy-paste attack

Table 8 compares the detectability of different approaches under copy-paste attacks, where each watermarked text contains 36 embedded bits within a 400-token sequence. Besides, Fig. 12 and Fig. 13 shows the detectability of MirrorMark against copy-paste attacks with 36 bits embedded in 400 tokens, where different m are compared. $m \in \{2, 3, 4, 6\}$ is corresponding to $H \in \{18, 12, 9, 6\}$ respectively.


 Figure 9: ROC across three languages over 200 tokens, where $m = 3$ and the number of positions $H=12$

● Tour_Bayes ■ Tour_Wmean ● Uniform ○ Bernoulli

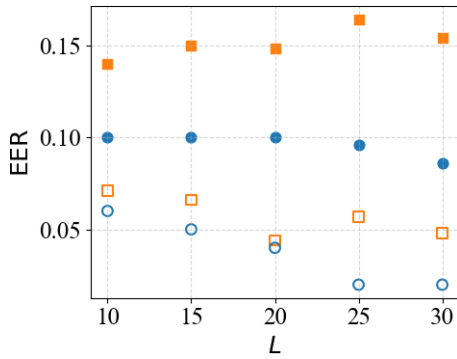


Figure 10: Empirical EER of tournament-based MirrorMark on Gemma-7B-it (Team et al., 2024) with ELI5 prompts (Fan et al., 2019), with token length $T = 200$ and temperature $\tau = 1.0$. $m = 1$ and $H = 1$.

Table 7: Perplexity of 200-token instruction-following responses on Gemma-7B-it with ELI5 prompts. We report the mean perplexity with a 90% bootstrap confidence interval. Bernoulli u is only applicable to tournament-based MirrorMark and only when $m = 1$.

	$m=1$		$m=3$
	Uniform	Bernoulli	Uniform
Non-watermark			1.7829 [1.7569, 1.8094]
Gumbel-max	1.8101 [1.7785, 1.8432]	—	1.7940 [1.7621, 1.8266]
Tour-Bayes	1.7784 [1.7493, 1.8079]	1.8208 [1.7882, 1.8541]	1.7986 [1.7681, 1.8300]

I.8. Ablation study for CABS

I.8.1. SENSITIVITY OF PARAMETERS

To analyze the sensitivity of CABS to its design parameters, we conduct a comprehensive ablation over the frame size f , context window W , and maximum frame expansion factor max_factor . Tables 9, 10, and 11 report results under insertion, deletion, and substitution attacks, respectively. For each attack, we consider edit ratios $\epsilon \in \{0, 0.2, 0.4\}$, where $\epsilon = 0$ corresponds to the no-attack setting.

Overall, the ablation results reveal clear and consistent trends across attack types. Setting $f = 3$ consistently

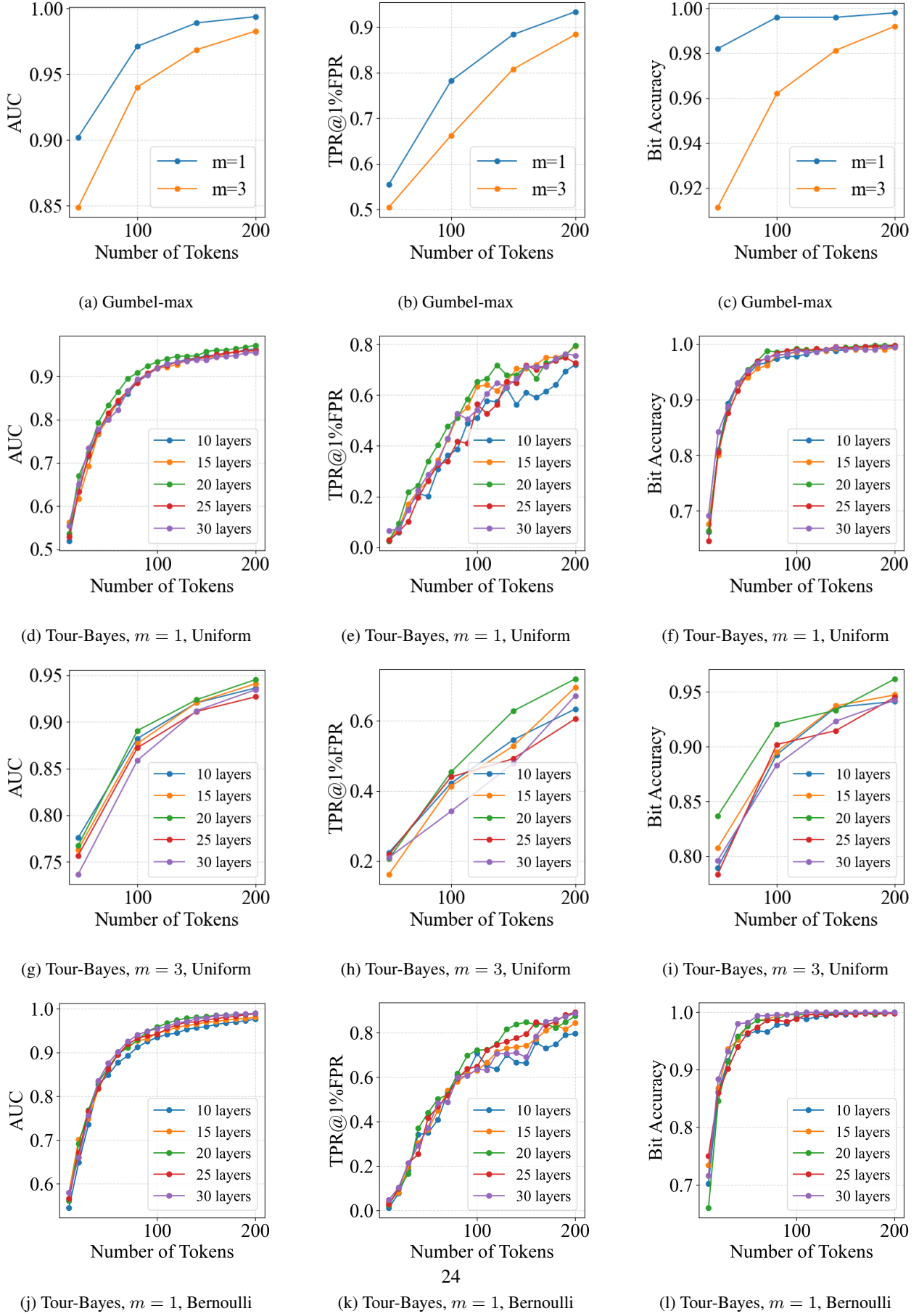


Figure 11: Detectability of MirrorMark on Gemma-7B-it and ELI5 prompts, with watermark of $m \in \{1, 3\}$ and $H = 1$ embedded in each response. The temperature is set to be 1.0

Table 8: Detectability for different approaches on 400 tokens with 36 bits embedded after copy-paste attack, where the edit fraction $\epsilon \in \{0.1, 0.3, 0.5\}$.

Method	$\epsilon = 0.1$			$\epsilon = 0.3$			$\epsilon = 0.5$		
	AUC	TPR@1%FPR	Bit Acc.	AUC	TPR@1%FPR	Bit Acc.	AUC	TPR@1%FPR	Bit Acc.
MPAC	0.9847	0.9025	0.9263	0.9729	0.8650	0.8725	0.9290	0.6075	0.7959
RSBH	0.9840	0.4275	0.6156	0.9386	0.0150	0.6181	0.7243	0.01	0.5825
StealthInk	0.9901	0.9100	0.8870	0.9636	0.6675	0.8213	0.8374	0.2575	0.7419
Tour-Wmean	0.9989	0.9980	0.9357	0.9932	0.9680	0.8750	0.9671	0.7560	0.7880
Tour-Bayes	0.9987	0.9960	0.9357	0.9944	0.9760	0.8750	0.9787	0.7920	0.7880
Gumbel-max	1.0	1.0	0.9801	1.0	1.0	0.9549	1.0	1.0	0.8986

achieves the highest bit accuracy and strong TPR@1%FPR under all attacks, indicating an optimal balance between robustness and effective token utilization. The context window $W = 4$ performs best or near-best across all edit ratios, capturing sufficient contextual information without overfitting to local perturbations. Similarly, `max_factor` = 1.5 yields the strongest robustness across edit rates, balancing frame-size flexibility and stability. These observations collectively justify the default configuration used in the main paper: $f = 3$, $W = 4$, `max_factor` = 1.5.

We further observe that different attack types affect detectability and bit recovery in distinct ways. Insertion primarily shifts token positions forward. Even at $\epsilon = 0.4$, MirrorMark maintains high detectability (AUC = 0.999, TPR@1%FPR = 0.992), while bit accuracy drops to 0.790, indicating that insertion mainly impairs bit recovery rather than WM/Non-WM separation. Deletion is the most adversarial attack, as it reduces the number of available tokens. At $\epsilon = 0.4$, AUC remains above chance, i.e., 0.939 and TPR@1%FPR degrades to 0.604, which arises not only from desynchronization of the token-to-position mapping but also from reduced detectability due to fewer surviving tokens. In contrast, substitution preserves sequence length and is the least destructive. At $\epsilon = 0.4$, MirrorMark sustains strong detectability, i.e., AUC=0.998, TPR@1%FPR=0.992, and relatively high bit accuracy, i.e., 0.75–0.78, confirming that CABS effectively absorbs localized perturbations.

I.8.2. THE EFFECT OF POSITION ALLOCATION SCHEDULERS ON WATERMARKING SCHEMES

To disentangle the contribution of mod-1 mirroring from that of position allocation, we conduct an ablation that systematically combines different position schedulers with different watermarking schemes. In particular, we incorporate the position schedulers used in MPAC and RSBH, which we denote as *NaiveHash* and *DPHash*, respectively. NaiveHash (MPAC, Section 3.2) seeds a PRF using the previous h tokens to randomly select a position, whereas DPHash (RSBH, Section 4.2) constructs a balanced token-to-segment mapping through a secret-key shuffle followed

by a dynamic programming procedure.

Because the DPHash table released in the official implementation of RSBH is constructed with $h = 1$, we evaluate performance under this setting in Fig. 15. In addition, since our main experiments use $h = 4$ by default unless otherwise noted, we also report results under $h = 4$ in Fig. 16. For both settings, we report the Gini coefficient⁵ in Fig. 14, which quantifies how balanced the token allocation is across positions, where lower values indicate more balanced allocation.

Across all configurations, CABS consistently achieves significantly lower Gini scores, approaching zero, indicating near-uniform token allocation across positions. This balanced allocation leads to substantial improvements in detectability for MirrorMark under both Tour-Bayes and Gumbel-max, with CABS outperforming NaiveHash and DPHash across all detection metrics. In contrast, for MPAC, the AUC and TPR@1%FPR of CABS are comparable to those obtained with NaiveHash and DPHash, while the bit accuracy of CABS is only slightly higher. This behavior is expected, as balanced allocation primarily improves the reliability of message decoding.

The difference between MirrorMark and MPAC stems from how positional evidence is aggregated. MirrorMark aggregates evidence from all positions, making it highly sensitive to positional imbalance. For example, consider a text of 100 tokens distributed across four positions as 85–5–5–5. In watermark text, the dominant position provides a strong signal for the correct message, whereas the remaining lightly populated positions contribute mostly noise. When combined in the final score, this noisy evidence dilutes the strong signal, making watermark and non-watermark score distributions harder to separate.

In contrast, MPAC is robust under the same allocation. The dominant position overwhelmingly votes for the correct message in watermark text, while non-watermark text remains approximately balanced across message candidates. Since MPAC retains only the maximum vote per position

⁵https://en.wikipedia.org/wiki/Gini_coefficient

Setting		AUC	TPR@1%FPR	Bit Accuracy
Varying f (with $W = 4$, max_factor=1.5)				
$\epsilon = 0.0$	$f = 1$	1.000	0.998	0.939
	$f = 2$	1.000	0.998	0.952
	$f = 3$	1.000	1.000	0.985
	$f = 4$	1.000	0.998	0.957
$\epsilon = 0.2$	$f = 1$	0.999	0.996	0.828
	$f = 2$	0.999	0.996	0.838
	$f = 3$	1.000	0.998	0.852
	$f = 4$	1.000	0.996	0.847
$\epsilon = 0.4$	$f = 1$	0.998	0.984	0.772
	$f = 2$	0.999	0.988	0.766
	$f = 3$	0.999	0.992	0.790
	$f = 4$	0.999	0.992	0.785
Varying W (with $f = 3$, max_factor=1.5)				
$\epsilon = 0.0$	$W = 1$	1.000	0.998	0.945
	$W = 2$	1.000	0.998	0.943
	$W = 3$	1.000	0.998	0.946
	$W = 4$	1.000	1.000	0.985
	$W = 5$	1.000	1.000	0.944
$\epsilon = 0.2$	$W = 1$	0.999	0.994	0.841
	$W = 2$	0.999	0.998	0.843
	$W = 3$	1.000	0.998	0.841
	$W = 4$	1.000	0.998	0.852
	$W = 5$	1.000	0.996	0.835
$\epsilon = 0.4$	$W = 1$	0.998	0.990	0.769
	$W = 2$	0.999	0.992	0.770
	$W = 3$	1.000	0.994	0.769
	$W = 4$	0.999	0.992	0.790
	$W = 5$	0.998	0.982	0.763
Varying max_factor (with $f = 3, W = 4$)				
$\epsilon = 0.0$	max_factor = 1.25	1.000	1.000	0.948
	max_factor = 1.50	1.000	1.000	0.985
	max_factor = 2.00	1.000	1.000	0.955
$\epsilon = 0.2$	max_factor = 1.25	1.000	0.996	0.850
	max_factor = 1.50	1.000	0.998	0.852
	max_factor = 2.00	1.000	1.000	0.839
$\epsilon = 0.4$	max_factor = 1.25	0.999	0.988	0.768
	max_factor = 1.50	0.999	0.992	0.790
	max_factor = 2.00	0.998	0.990	0.778

Table 9: Robustness of MirrorMark under insertion attacks with different CABS parameters, where $m = 2$, $H = 12$, and the number of tokens is 300.

		Setting	AUC	TPR@1%FPR	Bit Accuracy
Varying f (with $W = 4$, max_factor=1.5)					
$\epsilon = 0.0$	$f = 1$	1.000	0.998	0.939	
	$f = 2$	1.000	0.998	0.952	
	$f = 3$	1.000	1.000	0.985	
	$f = 4$	1.000	0.998	0.957	
$\epsilon = 0.2$	$f = 1$	0.998	0.988	0.683	
	$f = 2$	0.997	0.984	0.702	
	$f = 3$	0.999	0.988	0.700	
	$f = 4$	0.998	0.982	0.700	
$\epsilon = 0.4$	$f = 1$	0.939	0.604	0.464	
	$f = 2$	0.942	0.566	0.471	
	$f = 3$	0.946	0.566	0.472	
	$f = 4$	0.945	0.584	0.474	
Varying W (with $f = 3$, max_factor=1.5)					
$\epsilon = 0.0$	$W = 1$	1.000	0.998	0.945	
	$W = 2$	1.000	0.998	0.943	
	$W = 3$	1.000	0.998	0.946	
	$W = 4$	1.000	1.000	0.985	
	$W = 5$	1.000	1.000	0.944	
$\epsilon = 0.2$	$W = 1$	0.998	0.980	0.686	
	$W = 2$	0.999	0.990	0.689	
	$W = 3$	1.000	0.986	0.707	
	$W = 4$	0.999	0.988	0.700	
	$W = 5$	0.999	0.988	0.700	
$\epsilon = 0.4$	$W = 1$	0.956	0.580	0.476	
	$W = 2$	0.948	0.564	0.465	
	$W = 3$	0.947	0.600	0.481	
	$W = 4$	0.946	0.566	0.472	
	$W = 5$	0.949	0.592	0.453	
Varying max_factor (with $f = 3, W = 4$)					
$\epsilon = 0.0$	max_factor = 1.25	1.000	1.000	0.948	
	max_factor = 1.50	1.000	1.000	0.985	
	max_factor = 2.00	1.000	1.000	0.955	
$\epsilon = 0.2$	max_factor = 1.25	0.999	0.986	0.682	
	max_factor = 1.50	0.999	0.988	0.700	
	max_factor = 2.00	0.999	0.990	0.693	
$\epsilon = 0.4$	max_factor = 1.25	0.954	0.606	0.464	
	max_factor = 1.50	0.946	0.566	0.472	
	max_factor = 2.00	0.950	0.558	0.464	

Table 10: Robustness of MirrorMark under deletion attacks with different CABS parameters, where $m = 2$, $H = 12$, and the number of tokens is 300.

		Setting	AUC	TPR@1%FPR	Bit Accuracy
Varying f (with $W = 4$, max_factor=1.5)					
$\epsilon = 0.0$	$f = 1$	1.000	0.998	0.939	
	$f = 2$	1.000	0.998	0.952	
	$f = 3$	1.000	1.000	0.985	
	$f = 4$	1.000	0.998	0.957	
$\epsilon = 0.2$	$f = 1$	0.998	0.970	0.684	
	$f = 2$	0.997	0.984	0.710	
	$f = 3$	0.998	0.984	0.723	
	$f = 4$	0.997	0.984	0.709	
$\epsilon = 0.4$	$f = 1$	0.960	0.646	0.492	
	$f = 2$	0.945	0.644	0.504	
	$f = 3$	0.948	0.648	0.499	
	$f = 4$	0.957	0.622	0.486	
Varying W (with $f = 3$, max_factor=1.5)					
$\epsilon = 0.0$	$W = 1$	1.000	0.998	0.945	
	$W = 2$	1.000	0.998	0.943	
	$W = 3$	1.000	0.998	0.946	
	$W = 4$	1.000	1.000	0.985	
	$W = 5$	1.000	1.000	0.944	
$\epsilon = 0.2$	$W = 1$	0.998	0.968	0.703	
	$W = 2$	0.999	0.990	0.709	
	$W = 3$	0.997	0.984	0.709	
	$W = 4$	0.998	0.984	0.723	
	$W = 5$	0.997	0.984	0.690	
$\epsilon = 0.4$	$W = 1$	0.942	0.638	0.503	
	$W = 2$	0.933	0.574	0.494	
	$W = 3$	0.951	0.632	0.490	
	$W = 4$	0.948	0.648	0.499	
	$W = 5$	0.947	0.590	0.489	
Varying max_factor (with $f = 3, W = 4$)					
$\epsilon = 0.0$	max_factor = 1.25	1.000	1.000	0.948	
	max_factor = 1.50	1.000	1.000	0.985	
	max_factor = 2.00	1.000	1.000	0.955	
$\epsilon = 0.2$	max_factor = 1.25	0.998	0.978	0.708	
	max_factor = 1.50	0.998	0.984	0.723	
	max_factor = 2.00	0.998	0.982	0.709	
$\epsilon = 0.4$	max_factor = 1.25	0.949	0.610	0.486	
	max_factor = 1.50	0.948	0.648	0.499	
	max_factor = 2.00	0.951	0.624	0.482	

Table 11: Robustness of MirrorMark under substitution attacks with different CABS parameters, where $m = 2$, $H = 12$, and the number of tokens is 300.

and aggregates these maxima, lightly populated positions contribute little and do not introduce harmful noise. As a result, the detectability of MPAC remains stable even under highly uneven token allocation.

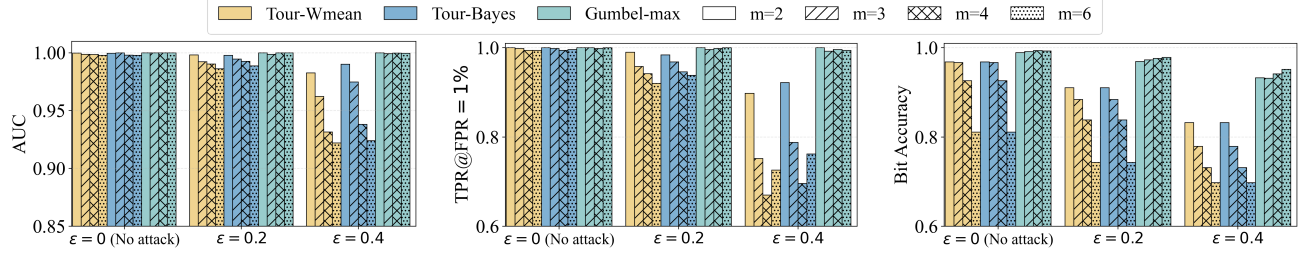


Figure 12: Detectability of MirrorMark against copy-paste attacks with 36 bits embedded in 400 tokens, where the edit fraction $\epsilon \in \{0, 0.2, 0.4\}$. To embed 36 bits, different m applies for various number of positions H , i.e., $m \in \{2, 3, 4, 6\}$ is respectively corresponding to $H \in \{18, 12, 9, 6\}$.

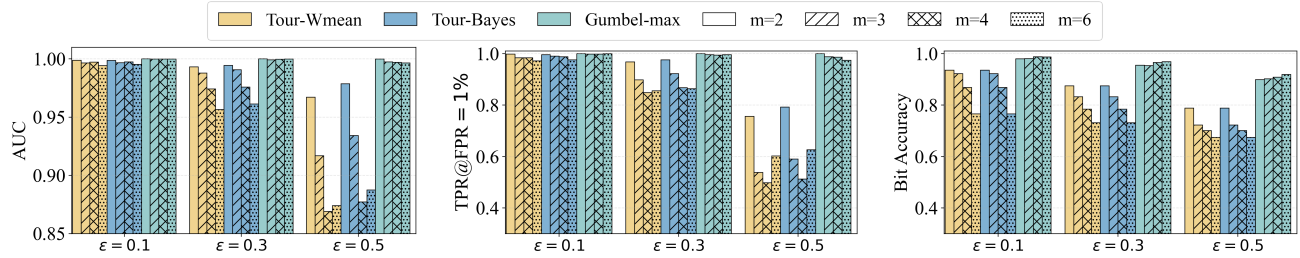


Figure 13: Detectability of MirrorMark against copy-paste attacks with 36 bits embedded in 400 tokens, where the edit fraction $\epsilon \in \{0.1, 0.3, 0.5\}$. To embed 36 bits, different m applies for various number of positions, i.e., the number of positions for $m \in \{2, 3, 4, 6\}$ is respectively, 18, 12, 9, 6.

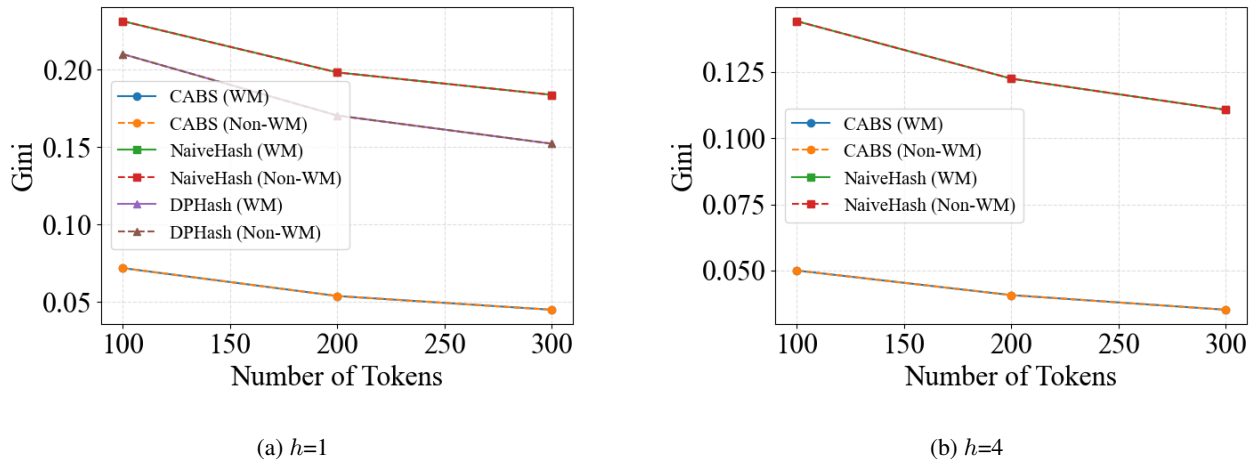


Figure 14: Comparison of token-allocation balance between different position scheduler. The setting is $m = 2$, $H = 12$, and the number of tokens is 300. The Gini coefficient is significantly lower (more balanced allocation) when using CABS, showing that CABS reduces position-allocation skew and improves uniformity.

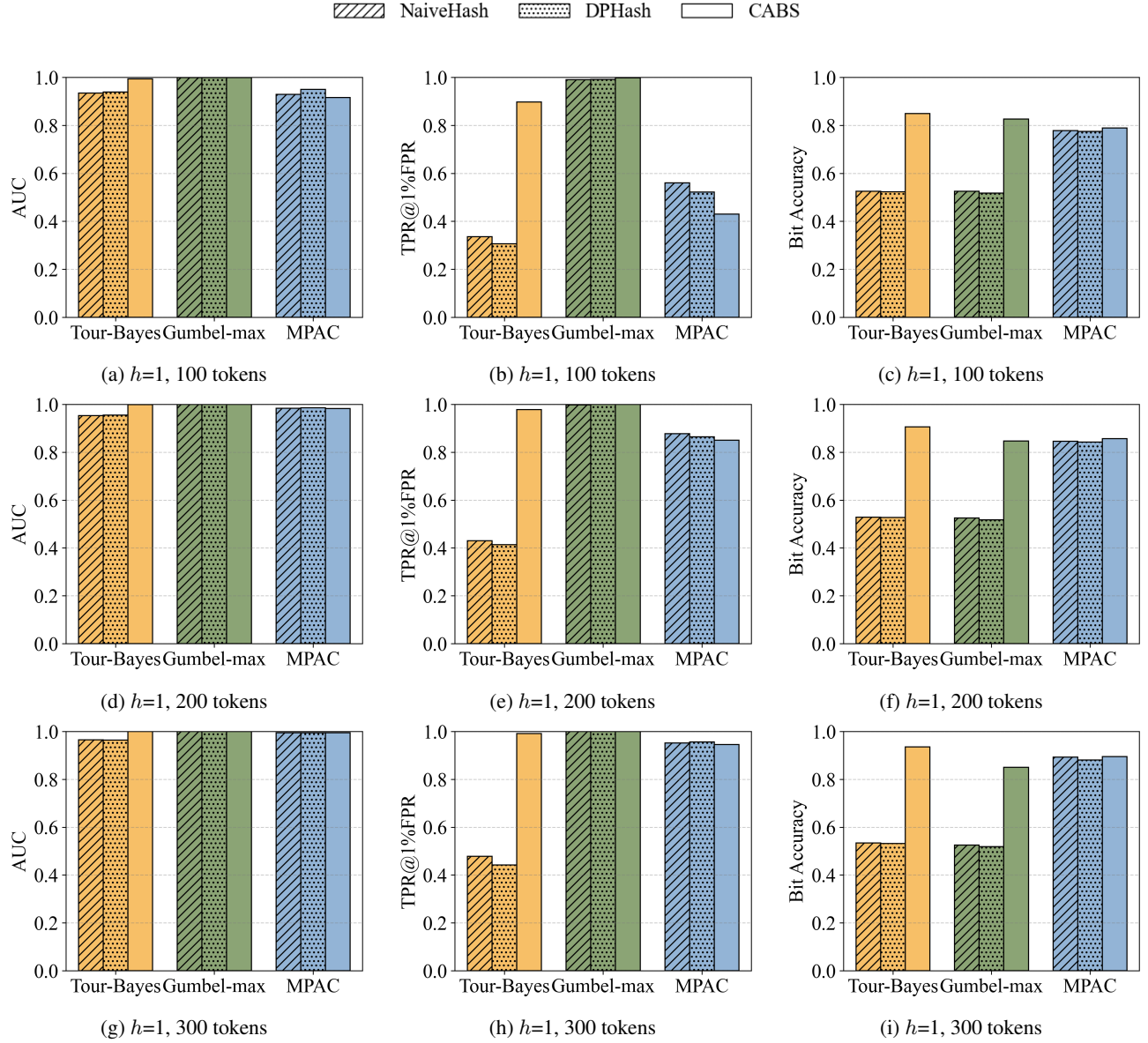
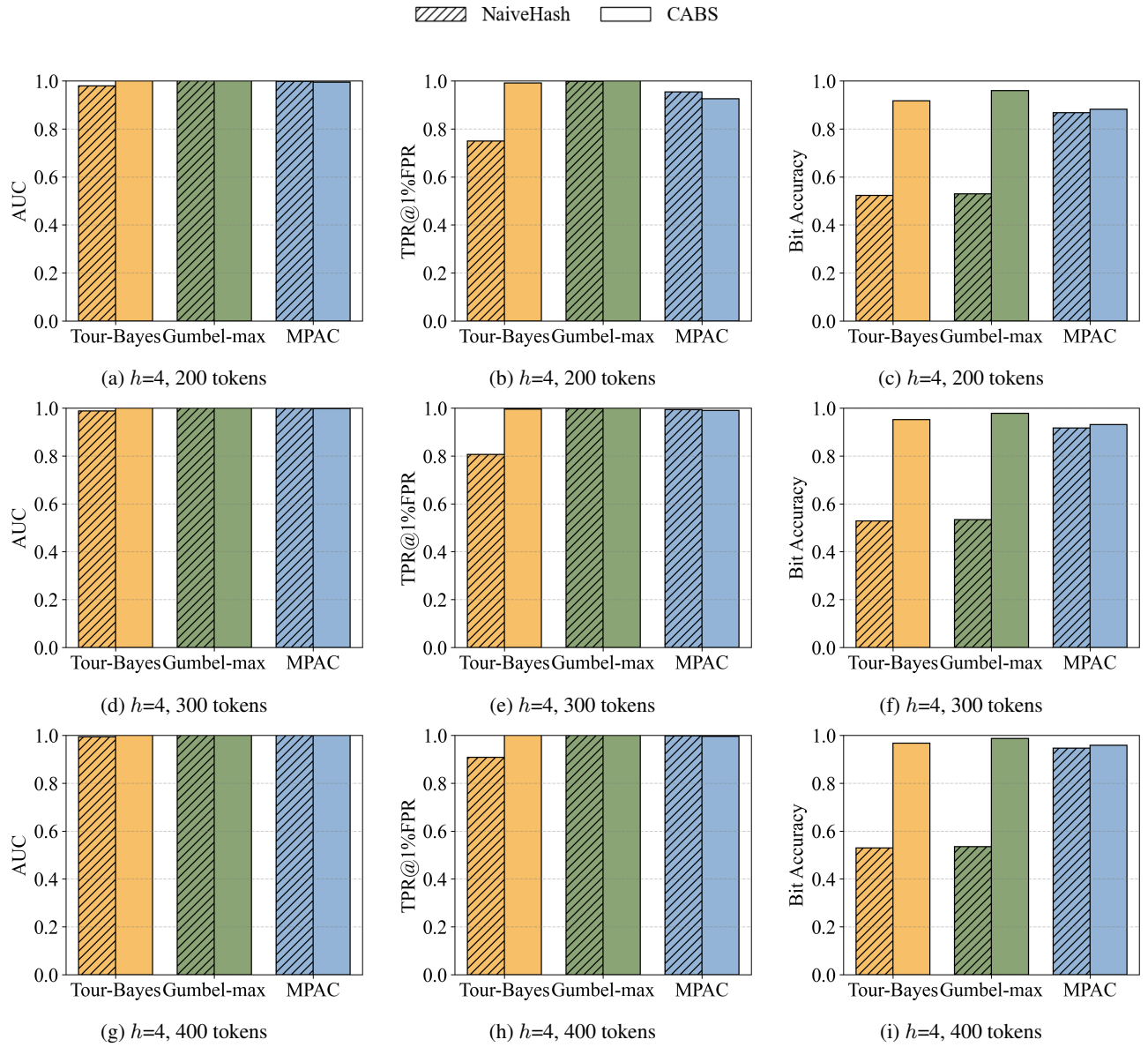


Figure 15: Detectability of MirrorMark with length of n-gram $h=1$. The setting is $m = 2$ and $H = 12$.


 Figure 16: Detectability of MirrorMark across $h=4$. The setting is $m = 2$ and $H = 12$.